Journal of Hydrology 617 (2023) 128991

Contents lists available at ScienceDirect

Journal of Hydrology

journal homepage: www.elsevier.com/locate/jhydrol

Research papers

Grid-based calibration of the WRF-Hydro with Noah-MP model with improved groundwater and transpiration process equations

Ioannis Sofokleous [a,*], Adriana Bruggeman [a], Corrado Camera [b], Marinos Eliades [a]

[a] Energy, Environment and Water Research Center (EEWRC), The Cyprus Institute, Nicosia, Cyprus
[b] Dipartimento di Scienze della Terra "A. Desio", Università degli Studi di Milano, Milan, Italy

ARTICLE INFO

This manuscript was handled by Marco Borga, Editor-in-Chief, with the assistance of Yadu Pokhrel, Associate Editor

Keywords:
WRF-Hydro
Noah-MP
Grid-based calibration
Nocturnal transpiration
Semi-arid
Conceptual groundwater model

ABSTRACT

The physically-based distributed WRF-Hydro modelling system, including the Noah land surface model with multiple parameterization options (Noah-MP) and the hydrological extension of the WRF atmospheric model (Weather Research and Forecasting model), has recently been widely used for water balance investigations, streamflow and coupled land–atmosphere simulations. Despite the multiple available physical parameterizations in the model, equations for simulating particular losses from the water balance are missing, and a grid-based calibration of distributed parameters across multiple watersheds has not been studied. To fill these gaps, this study aims: (i) to analyze the impact of soil, runoff, groundwater and vegetation parameters on water balance components; (ii) to improve baseflow and transpiration equations; and (iii) to test a grid-based calibration approach for distributed model parameters, using streamflow observations. The WRF-Hydro groundwater model was improved through the introduction of a groundwater loss factor and the Jarvis stomatal conductance model was modified to account for nocturnal transpiration. The grid-based calibration was performed for three parameters (infiltration, hydraulic conductivity and percolation) for 19 spatially-distributed classes, with the Parameter Estimation (PEST) software. The study area includes 31 small mountainous watersheds (5–115 km^2) in Cyprus, in the Eastern Mediterranean. A two-year period (2011–2013) was used for calibration and a five-year period (2013–2018) for the evaluation. The baseline model set-up overestimated streamflow, on average, by 50 % in 2011–2012 and more than 100 % in 2012–2013. Overall, streamflow and evapotranspiration (ET) could vary by about ±30 % from the baseline simulation, using different model parameters and model options. The simulation of groundwater losses as a function of groundwater level reduced total streamflow, on average, by 30 %. The use of the proposed Jarvis equation for nocturnal transpiration increased the total ET, on average, by 25 %. The grid-based approach facilitated the calibration of the distributed parameters over the area of the 31 watersheds. The median Nash-Sutcliff Efficiency (NSE) was 0.49 during calibration, but 0.02 in the drier evaluation period. The calibrated WRF-Hydro model reproduced the annual variability of ET and the improved groundwater and transpiration equations reduced the substantial streamflow overestimation of WRF-Hydro. The model performance during dry years demonstrated the need for representation of more processes that occur in semi-arid environments with ephemeral streams and are not included in WRF-Hydro and Noah-MP. The grid-based WRF-Hydro parameterization can be applied to the full study area for fully-coupled atmospheric-hydrologic simulations.

1. Introduction

Physically-based and spatially distributed hydrological models have evolved over the last decades to become complex modelling systems that can represent the spatial variability of the hydrometeorological processes in the environment. These models expand the capabilities of the simple lumped or conceptual hydrological models by simulating hydrological variables in the three-dimensional land-surface and subsurface space, based on physical model formulation (Maxwell et al., 2007). Distributed models fit in a broad spectrum of applications. They are used to simulate streamflow, to reproduce flood events induced by extreme weather using spatially variable precipitation datasets (Yucel et al., 2015; Sofokleous et al., 2021) and to improve our understanding of the interactions and feedbacks between the land surface and

* Corresponding author.
E-mail address: i.sofokleous@cyi.ac.cy (I. Sofokleous).

https://doi.org/10.1016/j.jhydrol.2022.128991
Received 14 July 2022; Received in revised form 19 November 2022; Accepted 12 December 2022
Available online 16 December 2022

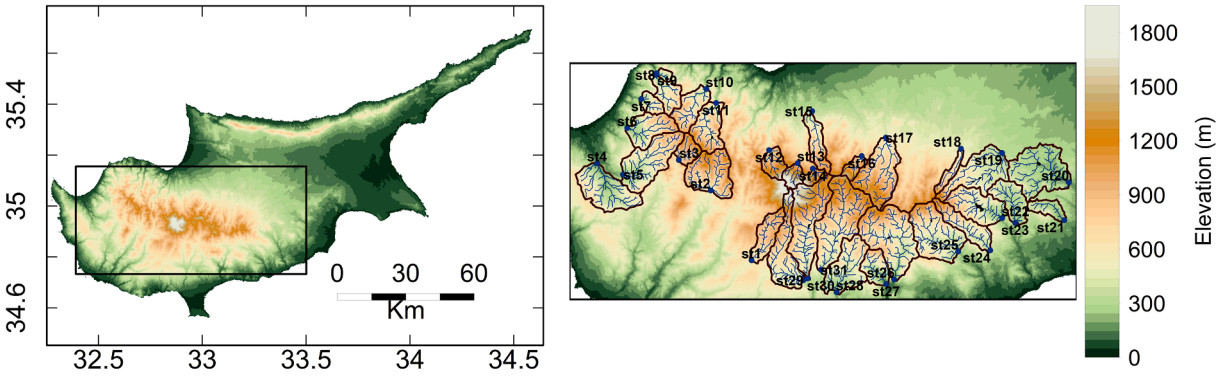

Fig. 1. The elevation map of Cyprus with the Troodos study domain enclosed with the black box (left) and the boundaries and outlets of the 31 watersheds of the study with the stream network and dams (right).

subsurface with the atmosphere, through fully coupled atmospheric-hydrologic model systems (Maxwell et al., 2011; Arnault et al., 2018; Rummler et al., 2019).

The community WRF-Hydro hydrological model (Gochis et al., 2018) is a physically-based, spatially distributed model, which is the core of the US National Water Model (NOAA, 2016) and which has gained remarkable attention in research in the last few years. Developed as the hydrological extension of the widely used Weather and Research Forecasting (WRF) model (Skamarock et al., 2019), WRF-Hydro is comprised of the Noah Land Surface Model (LSM; Ek et al., 2003) or the Noah-MP LSM (Noah LSM with multiple parameterization options; Niu et al., 2011; Yang et al., 2011), enhanced with lateral terrestrial water flow and a baseflow component. It can operate in a fully coupled mode with the atmospheric WRF model. WRF-Hydro simulates overland flow, lateral subsurface flow, flow in the channel network as well as inflow, storage and outflow from surface and groundwater reservoirs (Gochis et al., 2018).

Previous studies identified a number of model parameters to which WRF-Hydro simulated streamflow exhibits high sensitivity and which should be calibrated. Arnault et al. (2015) and Yucel et al. (2015) identified the infiltration parameter REFKDT in the surface runoff parameterization as the most impactful for streamflow simulations. Yucel et al. (2015) found a significant reduction of simulated peak flow with an increase of REFKDT from 1 to 2, with the suggested range of REFKDT being from 0.5 to 5, according to the authors. Arnault et al. (2015) added that, apart from streamflow, modeled monthly total precipitation and other water balance components, simulated with the fully coupled WRF-Hydro, are also sensitive to REFKDT at the spatial scale of $\sim 100 \times 100$ km^2. Other authors confirmed the sensitivity of REFKDT, highlighting its importance in flood forecasting (Givati et al., 2016; Zhang et al., 2020). Due to its impact on the percolation of the soil and subsequently on baseflow, particularly over mountain watersheds, the parameter that controls percolation to groundwater at the bottom of the soil profile (SLOPE) is also among the parameters that have been examined by numerous authors (Silver et al., 2017; Camera et al., 2020). Other commonly calibrated parameters in WRF-Hydro and related LSMs are the vertical and lateral hydraulic conductivities (Senatore et al., 2015) and the surface and channel roughness coefficients (Yucel et al., 2015; Arnault et al., 2018). For the roughness parameters, Yucel et al. (2015) found a significant impact on peak discharge magnitude and timing for flood events.

Studies focusing only on the LSM component of WRF-Hydro, in particular on the Noah-MP LSM, showed that the calibration of parameters that describe land surface processes can impact the total runoff amounts. Cuntz et al. (2016) suggested that LSM calibration should be made against both latent heat and runoff fluxes, as plant and soil properties affect both fluxes. Ingwersen et al. (2015) found that daily latent heat was underestimated by the Ball-Berry model (Ball et al., 1987), which is the default stomatal conductance model in Noah-MP. Zheng et al. (2019) found that the Jarvis stomatal conductance model (Jarvis, 1976) produces more realistic transpiration in arid environments, compared to Ball-Berry, through simulation of annual and seasonal evapotranspiration (ET) with different configurations of Noah-MP for the different climate regions of the conterminous United States. These authors also reported that the Jarvis model produced significantly higher transpiration, an additional 11 % of total precipitation, compared to the Ball-Berry scheme. Whitley et al. (2009) and Wang et al. (2020) reported the observation of nocturnal transpiration through sap flow measurements for different species. These authors proposed modifications of the Jarvis formula and calibration of the parameters of the four stress functions of the formula to better capture the daily, nocturnal and seasonal variability of transpiration. The partitioning of the surface energy and water balance to sensible and latent heat fluxes in Noah-MP was also found to be sensitive to the particular leaf area index (LAI) and green vegetation fraction (GVF) dataset used (Fang et al., 2018). This impact of plant parameters and parameterizations has not been addressed in the simulation of the water balance in previous WRF-Hydro studies.

WRF-Hydro is often calibrated and used for streamflow simulations in semi-arid Mediterranean environments for flood events (e.g. Silver et al., 2017; Camera et al., 2020) and for multi-month simulations (e.g. Senatore et al., 2015). A process that is not included in WRF-Hydro and may impact simulated streamflow through baseflow, particularly in dry areas, is groundwater flow across surface watersheds. Schaller and Fan (2009) used 30 years of streamflow data across 1555 basins in the United States and the Variable Infiltration Capacity model to estimate the partitioning of water balance in these basins. These authors found that the contribution of groundwater losses or gains in the water balance was significant. They suggested that geology plays the most important role for groundwater flows across basins, which are larger, in term of losses, in more arid regions. The occurrence of groundwater flow across watersheds was shown through isotope and hydrogeochemical sampling and modelling analyses for the Troodos area in the Eastern Mediterranean island of Cyprus by Christofi et al. (2020).

Despite the spatially distributed nature of WRF-Hydro, little to no attention has been given to a parameter calibration that is consistent with the spatial heterogeneity of the environment. The reason for this is that previous WRF-Hydro model versions did not easily allow the modeler to assign spatially variable values to a number of important model parameters. Givati et al. (2016) calibrated the infiltration parameter and hydraulic conductivity uniformly for a single watershed and then adjusted the calibrated values for subwatersheds. Silver et al. (2017) proposed a calibration of REFKDT by solving the model equation for infiltration for different soil texture types and observed values of hydraulic conductivity, soil moisture, runoff and precipitation. Rummler et al. (2019) assigned different values to the infiltration parameter, hydraulic conductivity and percolation parameter using information from land management maps. Yet, most of the WRF-Hydro studies assign

Table 1
The streamflow station codes, the area, and long-term (1980–2015) average precipitation (P), reference evapotranspiration (ET_o), runoff coefficient (RC), baseflow index (BFI) and the percent coverage of different geological types of the 31 watersheds.

Id	Area (km^2)	P (mm)	ET_o (mm)	RC (-)	BFI (-)	Sedimentary (%)	Vulcanic complex (%)	Diabase (%)	Ultramafic (%)	Gabbro (%)
st1	38.3	708	1203	0.11	0.79	69	5	22	0	4
st2	67.5	709	1224	0.22	0.72	0	0	100	0	0
st3	21.4	724	1163	0.21	0.75	0	0	100	0	0
st4	63.9	558	1274	0.04	0.65	100	0	0	0	0
st5	78.6	621	1251	0.13	0.74	29	17	54	0	0
st6	45.2	595	1222	0.10	0.74	0	4	96	0	0
st7	15.1	528	1211	0.14	0.89	0	0	100	0	0
st8	28.4	539	1237	0.14	0.77	0	0	96	0	4
st9	5.2	549	1233	0.12	0.84	0	0	92	0	8
st10	38.1	612	1247	0.20	0.82	0	0	100	0	0
st11	47.9	674	1262	0.24	0.79	0	0	100	0	0
st12	22.5	783	1096	0.31	0.89	0	0	17	17	67
st13	15.9	868	968	0.57	0.96	0	0	0	95	5
st14	10.2	837	1071	0.20	0.90	0	0	0	36	64
st15	32.7	533	1234	0.06	0.76	0	3	47	0	50
st16	13.6	710	1167	0.20	0.61	0	0	86	0	14
st17	78	613	1249	0.23	0.67	0	0	89	1	11
st18	14.1	526	1340	0.18	0.50	0	9	91	0	0
st19	74.2	459	1390	0.11	0.56	1	59	39	0	1
st20	93.8	405	1408	0.06	0.49	20	64	12	0	3
st21	20	412	1354	0.08	0.55	11	54	34	0	0
st22	61.2	517	1363	0.04	0.8	5	22	72	0	1
st23	39	443	1402	0.11	0.51	0	81	19	0	0
st24	43.3	543	1294	0.07	0.56	32	8	56	0	4
st25	86.7	559	1314	0.11	0.8	0	11	62	15	12
st26	109.7	599	1286	0.15	0.74	0	4	53	25	17
st27	30.5	515	1334	0.07	0.75	29	11	8	42	9
st28	66.8	534	1346	0.06	0.78	66	4	13	13	4
st29	67.5	669	1240	0.2	0.63	82	1	5	7	5
st30	98.9	738	1210	0.14	0.83	35	4	9	18	34
st31	114.7	657	1255	0.13	0.77	16	11	42	0	31
Area weighted averages		595	1276	0.14	0.72	20	14	48	7	11

parameter values uniformly over entire watersheds. A systematic and efficient approach to link the most important model parameters to landscape characteristics in a spatially distributed manner, as Hundecha and Bárdossy (2004) suggested, is currently missing.

This study aims to answer the following research question: Can the physically-based WRF-Hydro model simulate streamflow of small semi-arid mountain watersheds with an automated grid-based calibration based on the topography, land use and geology data of the study area, considering losses from groundwater and nocturnal transpiration. In light of this question, the objectives of this study are: (i) to examine the impact of soil, runoff, groundwater and vegetation parameters on annual streamflow, peak flows and total ET, (ii) to improve baseflow and transpiration equations and (iii) to test a grid-based calibration approach for spatially heterogeneous parameters. These objectives are implemented in 31 small watersheds in the Troodos Mountains on the island of Cyprus, in the Eastern Mediterranean. The changes in streamflow and water balance components due to alternative parameter values and parameterization options relative to a reference baseline model configuration are compared first for the two-year period from September 2011 to September 2013 (objective i and ii). The model with the modified groundwater and transpiration equations is then calibrated with an automated grid-based calibration of distributed parameters for the same two-year period. The calibrated model is evaluated for the period from October 2013 to September 2018 (objective iii).

2. Methodology

2.1. Study area and observational data

The study geographically focuses on 31 watersheds of Cyprus. Cyprus is an island with an area of 9251 km^2, located in the eastern part of the Mediterranean Sea and it has a Mediterranean climate. The 31 studied watersheds (st1 – st31) form a radial percolation system around Troodos, the main mountain range of the island (Fig. 1). Daily streamflow, recorded by the Water Development Department of Cyprus at the outlets of the 31 watersheds, is used in this study for the evaluation of daily totals of WRF-Hydro streamflow. The areas of the 31 watersheds range from 5 to 115 km^2. Long-term average precipitation, reference evapotranspiration (ET_o), runoff coefficients (RC), baseflow indices (BFI) and percent coverage of different geological formations of the 31 watersheds are shown in Table 1. The precipitation over the watershed areas was derived from gridded daily precipitation (Camera et al., 2014; Sofokleous et al., 2021). The ET_O was computed with the Hargreaves's equation (Hargreaves and Samani, 1985) using gridded daily temperature data for the period 1980–2010 (Camera et al., 2014). The RC was computed as the fraction of total annual streamflow to total precipitation. Daily baseflow was extracted from the daily streamflow with the PART hydrograph separation method (Rutledge, 1998) and the BFI was computed as the fraction of total annual baseflow to total annual streamflow.

Geologically, Troodos is constituted by an ophiolite complex with plutonic, intrusive and volcanic rocks and chemical sediments. Most of the rocks of the ophiolite, especially the gabbro within the central plutonic sequence on the upper hillslope, are faulted, highly fractured and brecciated, thus forming fractured aquifers or aquifer systems favoring infiltration (Udluft et al., 2006). Troodos has mostly lithic leptosols with a stony gravelly texture and a high variability in soil depth, from very shallow (0–10 cm) up to about 100 cm (Camera et al., 2017).

The study area is to a large extent covered by natural vegetation (70 %), comprised mostly by sclerophyllous vegetation and coniferous forests and to a lesser extent by crops cultivated on dry stone bench terraces (Zoumides et al., 2017). The annual average ET to precipitation ratio is 76 %, according to long-term observations (2014–2020) of ET components on a pine forest monitoring site near the outlets of two of the studied watersheds (st16 and st17) (Eliades et al., 2018a; Eliades, personal communication). About 15 % of the transpiration is nocturnal

transpiration (Eliades et al. 2018b). These long-term annual average ET observational data are used to evaluate and adjust modeled ET in Noah-MP with WRF-Hydro in this study.

2.2. Model description and new model equations

The WRF-Hydro modelling system (Gochis et al., 2018) is a distributed physically-based hydrologic model developed at the National Centre for Atmospheric Research. It simulates terrestrial hydrologic processes, i.e., surface, subsurface and channel flow, and enables hydrologic-atmospheric coupled modelling. The WRF-Hydro modelling system contains the following six components: (i) the land surface parameterizations of Noah-MP LSM, which control the vertical water and energy fluxes in the soil and on the land surface; (ii) an overland flow module; (iii) a subsurface flow module; (iv) a channel flow module; (v) a reservoir storage and flow module; and (vi) a conceptual baseflow module, which controls groundwater storage and fluxes. The WRF-Hydro v5.1 model version is used in this study.

The meteorological forcing data required by WRF-Hydro are incoming shortwave and longwave radiation, specific humidity, air temperature, surface pressure, near surface wind components and precipitation rate. In addition to the vegetation (MPTABLE.TBL), soil (SOILPARM.TBL) and global parameters (GENPARM.TBL) for the stand-alone Noah-MP LSM, Noah-MP with WRF-Hydro require parameters for the lateral routing. These include overland roughness, hydraulic conductivity in the lateral direction, as well as parameters for the channel and reservoir routing modules and for the groundwater bucket of WRF-Hydro. In addition, a number of Noah-MP land use, soil texture dependent and global parameters can be assigned spatially distributed values. All parameters are described in detail in Gochis et al. (2018).

2.2.1. Groundwater bucket loss factor

The equation for the groundwater bucket baseflow in WRF-Hydro v5.1 is:

$$Q_{bucket,out} = Coeff \bullet \left(e^{Expon\frac{Z}{ZMAX}} - 1\right) \quad \text{if } Z <= ZMAX$$
$$Q_{bucket,out} = Q_{bucket,in} + Coeff \bullet \left(e^{Expon\frac{Z}{ZMAX}} - 1\right) \quad \text{if } Z > ZMAX \tag{1}$$

where $Q_{bucket,out}$ (m^3s^{-1}) and $Q_{bucket,in}$ (m^3s^{-1}) are the conceptual bucket model outflow and inflow at a given model time step, Z (m) is the depth of water stored in the bucket and ZMAX (m) is the maximum water depth in the bucket. Parameters Coeff (m^3s^{-1}) and Expon (-) control the response of the conceptual bucket. The initial value of Z is set at the beginning of the simulation period. The depth of the water in the bucket (Z) for a defined gridded domain is adjusted by the total percolation ($Q_{bucket,in}$) of all grid cells of the gridded domain. The extent of the contributing gridded domain to a bucket is defined by the user. In this study, the contributing gridded area is defined to be the same as the surface watershed, for each of the 31 watersheds.

One novelty of this study is the incorporation of a loss factor in the baseflow routine of WRF-Hydro. The loss factor can represent groundwater losses from surface watersheds, as observed in the study area, and reduce the overestimation of baseflow, as seen in the baseline simulation experiments for the studied watersheds (Section 3.1.1). The modified equation of the groundwater bucket is:

$$Q_{bucket,out} = Coeff \bullet (1 - L_{fac}) \bullet \left(e^{Expon\frac{Z}{ZMAX}} - 1\right) \quad \text{if } Z <= ZMAX$$
$$Q_{bucket,out} = Q_{bucket,in} + Coeff \bullet (1 - L_{fac}) \bullet \left(e^{Expon\frac{Z}{ZMAX}} - 1\right) \quad \text{if } Z > ZMAX \tag{2}$$

where L_{fac} (-) is a dimensionless loss factor, ranging between 0 and 1, which quantifies a baseflow reduction from the bucket model, as a function of the water level in the bucket. Parameter L_{fac} represents the amount of groundwater losses from the specified surface watershed, which can occur in fractured formations or groundwater systems where only part of the total percolation contributes to the watershed's baseflow.

2.2.2. Nocturnal transpiration

The equations of the Jarvis-based stomatal conductance model in WRF-Hydro are based on the empirical stomatal conductance model proposed by Jarvis (1976), which is still widely used. The canopy stomatal resistance (r_s; sm^{-1}) can be computed at any environmental condition, according to Chen et al. (1996), and is given by the following equation:

$$r_s = rs_{min} \bullet (F_1F_2F_3F_4)^{-1} \tag{3}$$

where rs_{min} (sm^{-1}) is the vegetation-type dependent minimum stomatal resistance, corresponding to the value of canopy resistance at optimal environmental conditions for transpiration. The value of rs_{min} is defined for different vegetation types in the NOAHMP.TBL model input Table. F1, F2, F3 and F4 are four stress functions representing the effects of solar radiation, vapor pressure deficit, canopy air temperature and soil moisture, respectively, each ranging from 0 to 1. The model equation of the stress function F_1 is:

$$F_1 = \frac{r_{smin}/r_{smax} + f}{1 + f} \quad \text{where} \quad f = 0.55\frac{R_s}{R_{gl}}\frac{2}{LAI} \tag{4}$$

where r_{smax} is the maximum canopy resistance, which corresponds to the cuticular resistance of the leaves and a value of 5000 sm^{-1} is a representative value for many trees (Dickinson, 1984), R_s (Wm^{-2}) is the intensity of direct solar radiation and R_{gl} is a fitting parameter for the radiation response (F_1), ranging between 30 and 100 Wm^{-2} and can be vegetation-type specific (Noilhan and Planton, 1989). Appendix A contains the full equations for the Jarvis model.

The incorporation of a nocturnal transpiration component, based on Whitley et al. (2009) and Wang et al. (2020), in the Jarvis model in the Noah-MP code of WRF-Hydro, is the second novelty of the study. The ET underestimation, as seen in initial simulation experiments (Section 3.1.1), could be reduced by adding the nocturnal transpiration component. The equation that replaces Eq. (4) is:

$$F_1 = \left(\frac{R_s + k_1k_r}{R_m}\right) \bullet \left(\frac{R_m + k_1}{R_s + k_1}\right) \tag{5}$$

where R_m is the maximum solar radiation intensity at the latitude of the study area (~1000 Wm^{-2}), and k_1 (Wm^{-2}) and k_r (-) are two fitting parameters that describe the curvature of the radiation response. Trial-and-error runs were performed to adjust k_1 and k_r such that the annual magnitude of transpiration increased by 15 %, close to the locally observed nocturnal transpiration fraction to total transpiration (Eliades et al., 2018b). The increase in transpiration with adjusted parameters was examined relative to the transpiration obtained with kr = 0 in Eq. (5), which corresponds to zero nocturnal transpiration. The selected parameter values were 1 Wm^{-2} for k_1 and 0.5 for k_r. However, further calibration should be done on the Jarvis equation and the nocturnal component to match the diurnal transpiration patterns.

2.2.3. LAI and dynamic vegetation

The average leaf area index over a grid cell (LAI_{cell}) in WRF-Hydro is given by:

$$LAI_{cell} = GVF \bullet LAI \tag{6}$$

where LAI is the prescribed vegetation-type dependent leaf area index or the dynamically predicted leaf area index of the vegetation in the grid cell and GVF is the green vegetation fraction of the grid cell. The

values of LAI and GVF are controlled by the option for Dynamic Vegetation (DVEG) of Noah-MP. In WRF-Hydro, six DVEG options are available. Three DVEG options (2, 5 and 6) predict LAI dynamically with the Ball-Berry stomatal conductance model (Ball et al., 1987) and the other three options (1, 3 and 4) use tabulated, vegetation-specific monthly LAI values and can be used with any stomatal conductance model. The current study compares the performance of the Ball-Berry and Jarvis stomatal conductance models and for this reason, the focus here is on DVEG options that can be used with both conductance models, i.e., 1, 3 and 4. For the three options, the monthly LAI values are read from the NOAHMP.TBL model input table for the different land use classes. For DVEG option 1, the GVF has prescribed monthly values, which are derived from the MODIS dataset. For DVEG option 4, the GVF is the maximum of the 12 months of the MODIS-derived data, year-round. The equation for GVF for DVEG option 3 is based on Norman et al. (1995):

$$GVF = 1 - e^{-b \bullet LAI} \quad (7)$$

where b is the extinction coefficient and has a value of 0.52 in model code. Eq. (7) is part of the gap fraction theory by Larcher (1995), which implies that there is a light attenuation following an exponential decay with increasing canopy depth (Gigante et al., 2009). According to Larcher (1995) different land uses can have different extinction coefficients.

In addition to the above options, satellite-derived monthly LAI values of the Copernicus Global Land Service were tested for this study. The new LAI values were obtained by extracting the monthly Copernicus LAI for the year 2018 at 1-km for each land use type based on the gridded land use map (Section 2.3.2). These computed monthly values replaced the default monthly LAI in MPTABLE.TBL. Following the update of LAI, the GVF was set to a globally constant value equal to 1. The selection of 1 for GVF was based on the fact that satellite-derived LAI corresponds to pixel-average values of the vegetation density, making GVF redundant (Gutman and Ignatov, 1998). With the updating of the prescribed LAI values, the monthly prescribed stem area index values were replaced by 10 % of the LAI values, as assumed by the model. Appendix B contains the default and updated LAI values.

2.3. Model set-up and parameterization

2.3.1. Watershed delineation and atmospheric forcing

The 31 studied watersheds were delineated on a 100-m routing grid using the WRF-Hydro GIS-preprocessor (ArcMap WRF-Hydro GIS preprocessor v5.1.1) and the 25 m Digital Elevation Model for Cyprus from the Geological Survey Department of Cyprus. The Noah-MP LSM grid was generated using the WRF model preprocessing system (WPS; Skamarock et al., 2019) with spatial resolution at 1-km. The domain for lateral routing of WRF-Hydro and the domain for the simulation of land surface vertical fluxes of Noah-MP cover the Troodos mountain range (Fig. 1). Nine dams located upstream of eight streamflow stations in the study area were incorporated in the routing grid (Appendix D). The default MODIS land cover, with USGS land use categories, at approximately 1-km resolution was replaced by the Corine Land Cover (CLC) dataset, at 100-m resolution. The CLC dataset was reclassified to USGS land categories, as required by the model, according to Pineda et al. (2004), and is presented in Appendix B.

The meteorological forcing of the Noah-MP LSM in this study consists of the output of the WRF atmospheric model, except precipitation, which was obtained from the spatial interpolation and temporal disaggregation of precipitation gauge observations based on the methods described in Camera et al. (2014) and Sofokleous et al. (2021). The WRF-Hydro time step for routing was set to 10 s and the time step for Noah-MP was set to 30 min, the same as the temporal resolution of the atmospheric forcing and the model output time step. From the model output, 30-min streamflow and the annual totals for the water balance components of soil evaporation, canopy interception and transpiration and soil moisture storage change were extracted for the model evaluation.

2.3.2. Land surface classes

The values of spatially-distributed model parameters were directly related to the physical characteristics (land use, topographic slope and geology) of each grid cell. The infiltration parameter REFKDT in the surface runoff parameterization of WRF-Hydro was assigned spatially variable values based on nine land surface classes, which are a combination of three land uses and three topographic slope classes. The resulting nine land surface classes are shown in Fig. 2. The three land use classes were specified from the corresponding three dominant land uses in the study area. The three classes are the coniferous forest, the shrubland areas and the agricultural land. The remaining classes, each covering <3 % of the total area, were integrated in the three classes (see Table B1 Appendix B). The three topographic slope classes that were considered are flat to nearly flat terrain (<5%), moderate slopes (5–10 %) and steep slopes (greater than10 %). The three slope classes, cover areas of 32 %, 46 % and 22 %, respectively. The assumptions used for assigning values to REFKDT for different land surface classes were that infiltration capacity increases, and thus REFKDT increases, with decreasing topographic slope and with increasing ground cover, such as with natural vegetation as opposed to managed agricultural land.

2.3.3. Geological and soil type classes

Model parameters relevant to the soil and bedrock properties were linked to the geological formations of the study area. For the present geological formations over the 31 watersheds, five geological classes are defined (Fig. 2). The percolation controlling distributed parameter SLOPE was assigned values from 0 to 1 based on the permeability of these five classes. According to Udluft et al. (2006), basal group, diabase, gabbro and plagiogranite have the highest permeability values of all ophiolite rocks, whereas the vulcanic complex, found at the foothills of Troodos, has low permeabilites. The spatial distribution of the soil texture classes was the same as for the geological classes because the soil texture map for the mountainous part of Cyprus is characterized by high uncertainty (Camera et al., 2017).

2.4. Impact of model parameters and parameterization options on model outputs

The impact of model parameters and model parameterization options on annual total streamflow, annual total ET and peak flow (three-day total discharge around the date with annual peak flow) for two hydrological years (2011–2013) was examined. This impact was quantified with the relative change of each model output ($\Delta SIM_{par.i}$), which was computed as follows:

$$\Delta SIM_{par.i} = \frac{SIM_{par.i}}{SIM_{baseline}} \quad (8)$$

where $SIM_{par.i}$ is the model output variable computed with a certain parameter value or model parameterization option (par.i) and $SIM_{baseline}$ is the same variable obtained with the baseline parameter set. These relative changes were computed for all 31 watersheds.

The parameter values were tested assigning the same parameter value across the domain (Test value 1 or Test value 2 in Table 2). The parameter values for the impact analysis were selected to be the minimum and maximum of the range of values specified in the model parameter tables (Section 2.2). The parameterization options (DVEG, LAI, CANRES, RS.noc) were tested for one or two different settings. The selected parameters used in the analysis are parameters often reported in previous WRF-Hydro studies and vegetation parameters and parameterizations. The impact, however, of a larger number of parameters than those listed in Table 2 was examined with initial simulation experiments (results not shown). For soil texture dependent parameters, these

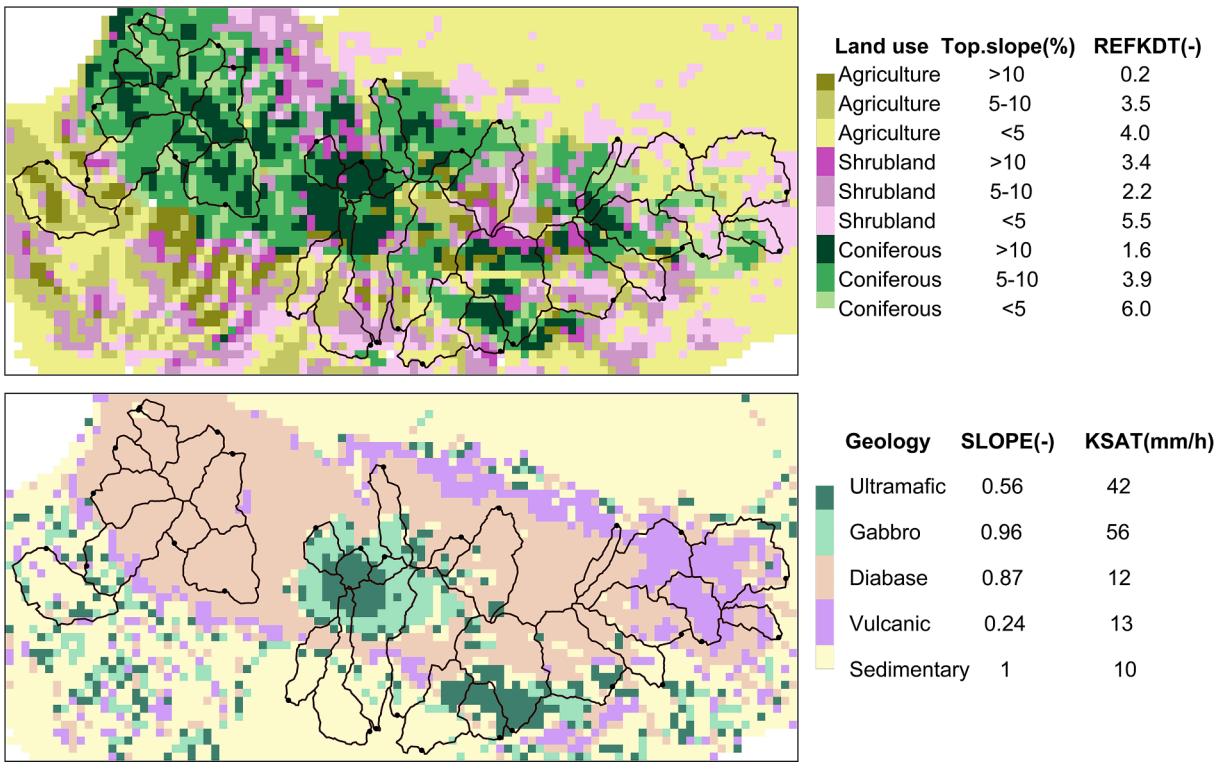

Fig. 2. Map of the WRF-Hydro domain with the boundaries of the 31 watersheds and the nine 1-km land surface classes representing three land uses and three topographic slopes (top) and the five geological classes (bottom). The final PEST calibrated values (see Section 3.2.1) for REFKDT for each land surface class are in the last column of the legend (top) and for SLOPE and KSAT for each geology class in the last two columns of the legend (bottom).

experiments showed that some parameters had similar impact and for this reason, their number was reduced for this study. The Ball-Berry parameters were found to lead to minor changes in the model outputs and they were also omitted.

The baseline parameterization is the same as the default WRF-Hydro configuration, but with the modifications of the parameter values described in this section, which were made to represent local environmental conditions. The baseline REFKDT was assigned spatially variable values based on the nine land surface classes (Section 2.3.2). REFKDT ranged, for the three topographic slope classes, from 2 to 4 for the agricultural land use, from 2.5 to 4.5 for shrubland and from 3 to 5 for the coniferous forest. The baseline percolation parameter (SLOPE) values ranged from 0.1 to 1. The soil physical properties were related to the five geological classes (Section 2.3.3). For soil properties, the baseline values were set as the default values, from SOILPARM.TBL model input file. The groundwater bucket baseline parameters are specified in Section 2.5.

Except for the REFKDT and SLOPE parameters, the impact of the soil texture properties was examined for the parameters of porosity (SMCMAX) and hydraulic conductivity (KSAT). The values tested for the soil parameters were set equal to the minimum and maximum of the range of values of the 13 soil textures specified in the Noah-MP SOILPARM.TBL file. The parameter for overland roughness (OV_ROUGH2D) ranged between the minimum and maximum default values of the 22 land-use dependent values specified in the HYDRO.TBL model file. The default 2-m soil depth in WRF-Hydro was set to the smaller value of 1-m, which is more representative of the generally shallow soils on the slopes of Troodos Mountains (Camera et al., 2017). The effects of re-initialization of the water depth in the GW bucket at the start of the second hydrological year (Z_{ini}) was examined. The Z_{ini} option allows to remove excess water from the GW bucket at the end of a hydrologic year. The groundwater loss factor in the baseflow bucket model equation (L_{fac}; Section 2.2.1) was tested as an alternative to the Z_{ini} option.

The second half of Table 2 presents the vegetation related model parameters and parameterization options. The baseline stomatal conductance model used for the study is the Ball-Berry model, which is the default in WRF-Hydro. The USGS land-use based monthly LAI values and the yearly maximum, MODIS-derived GVF comprise the baseline values for the vegetation density. The impact of the various options (DVEG) for the description of vegetation density (LAI and GVF), as introduced in Section 2.2.3 was examined. The impact of the Jarvis-based model for stomatal conductance was also examined, along with changes of the values of the Jarvis model parameters and the change of the Jarvis radiation component to account for nocturnal transpiration (Section 2.2.2).

2.5. Groundwater bucket parameters

One major characteristic of baseflow for the majority of the Troodos streams, as ephemeral, is the zero baseflow in the summer. Scatterplots of the long-term baseflow indices, i.e., the long-term average and maximum BFI with the relative coverage of different geological classes in each watershed (Table 1) did not show a relation between the two. For this reason, the groundwater parameters could not be related to the geological characteristics across the model domain and parameters ZMAX and L_{fac} were manually calibrated per watershed. Parameter Coeff of the GW bucket model (Section 2.2.1) was set to two times the average non-zero watershed baseflow for 28 watersheds, for the baseline parameter set. Three watersheds (st12, st13 and st14), which have a BFI equal or larger than 0.89 were assigned a value equal to 10 times the average non-zero daily baseflow of the watershed. Parameter Expon was set equal to 0.693 for the baseline parameterization, which corresponds to bucket outflow equal to the Coeff when the bucket is full.

2.6. Grid-based calibration with PEST

The spatially distributed model parameters, which were selected based on the results of the impact analysis (Section 3.1.2 and Section

Table 2
Parameters of WRF-Hydro for runoff, soil, groundwater (GW) bucket and vegetation used to examine the parameter impact on total streamflow, peak flow and total evapotranspiration.

Parameter Name	Parameter description	Baseline value	Test value 1	Test value 2
Runoff parameters				
REFKDT (-)	Infiltration parameter	2–5	0.5	5
OVROUGH (-)	Manning's roughness for overland flow	0.025–0.2	0.025	0.2
Soil parameters				
SLOPE (-)	Percolation parameter	0.1 – 1	0	1
KSAT ($mm \cdot h^{-1}$)	Hydraulic conductivity	9–50	4	168
SMCMAX (m^3/m^3)	Soil porosity	0.34–0.48	0.34	0.48
Soil (cm)	Soil column depth	100	125	
GW bucket parameters				
ZMAX (mm)	GW bucket maximum depth	Average long term baseflow per watershed	Max Q_b (maximum long term baseflow per watershed)	
Z_{ini} (mm)	GW bucket initial water depth	Default (Z not re-initialized in HY2[1])	ON (Z re-initialized in HY2 as 0 or 0.1 of the final Z in HY1[1])	
L_{fac} (-)	GW bucket loss factor	0	0.1	
Vegetation parameters				
DVEG	Option for dynamic vegetation (GVF)	4 (Yearly maximum GVF)	1 (Monthly GVF)	3 (GVF = f (LAI))
LAI	Leaf area index	monthly USGS land-use based[2]	Copernicus (Satellite-derived LAI[3] and GVF = 1)	
CANRES	Canopy stomatal resistance model	Ball-Berry	Jarvis	
CH20P (mm)	Maximum canopy interception per class LAI	0.1	0.5	
RS.noc	Solar radiation stress function in Jarvis model with nocturnal component or not	Default (no nocturnal component)	ON (With nocturnal component)	
TOPT (℃)	Optimal transpiration temperature in Jarvis model	25	20	
HS (-)	Parameter in vapor pressure deficit stress function in Jarvis model	35–47	35	
B (-)	Parameter in temperature stress function in Jarvis model	0.0016	0.0004	

1 HY1 and HY2 refer to hydrologic year 1 (Sep 2011 - Oct 2012) and hydrologic year 2 (Sep 2012 - Oct 2013).
2 Monthly land-use dependent LAI specified in NOAHMP.TBL input file of WRF-Hydro.
3 Monthly LAI extracted from Copernicus satellite for different land use classes, replacing default values in NOAHMP.TBL.

3.1.3), were calibrated for the land surface, soil and geology classes using the Parameter Estimation (PEST) calibration software (Doherty 2020). The calibrated parameter ranges were selected based on the ranges of the prescribed values for these parameters in the WRF-Hydro and Noah-MP input files. For each land surface class and geology class, the calibration range was further confined to a smaller range of values representative for the specific class, as described in Section 2.3.2 and Section 2.3.3.

The model parameter optimization, simultaneously for the 31 watersheds, was based on the minimization of the following objective function:

$$\Phi = \sum_{i}^{N_{obs}} (w_i r_i)^2 \quad (9)$$

where N_{obs} is the total number of observations, i.e., daily streamflow of 31 watersheds, w is the weight of each observation i, and r is the residual (difference between model value and observation value). The observation weights are set equal to zero or one, with the value of zero used for missing observations.

The PEST optimization algorithm is based on the least squares function and the Gauss-Marquardt-Levenberg method (Doherty, 2015). The PEST "estimation" mode was used with singular value decomposition, the latter guarantying numerical stability in the calibration process (Doherty, 2020). The streamflow observations of the 31 watersheds were grouped into 31 groups. The 31 watershed components in the objective function were assigned weights, using the PWTADJ1 utility of PEST, such that, based on the residuals obtained for the initial parameter values, the contribution to the objective function by each observation group will be equal. This avoids a dominance of the objective function value by the watersheds with the largest errors (Doherty, 2020). The automatic calibration with PEST is based on the iterative behavior of the PEST algorithm. This means that the calibration is made up of multiple PEST iterations, with each iteration comprised of multiple WRF-Hydro model runs with different sets of initial parameter values. This attribute of PEST limits the possibilities for selecting a locally optimum solution of calibrated parameter set as a globally optimum. The automatic calibration was terminated when PEST failed to lower the objective function for three consecutive iterations, as suggested in Doherty (2020).

2.7. Simulation period and evaluation metrics

The calibration and evaluation period, referred to as 2011–2013 and 2013–2018, cover the sequence of hydrologic years from October 2011 to September 2013 and from October 2013 to September 2018, respectively. The simulation period for the examination of the parameter impact on model outputs is the same as the calibration period. Following the adjustment of model parameters and options, based on the impact analysis (Section 3.1.2 and Section 3.1.3), and the PEST calibration of the distributed parameters (Section 3.2.1), the model was evaluated for both the two-year calibration period and the five-year evaluation period with four evaluation metrics (Section 3.2.2). These metrics are the Nash-Sutcliffe Efficiency (NSE; Appendix E), the Kling-Gupta Efficiency (KGE; Appendix E), the Mean Absolute Error (MAE) and the percent total bias. The individual annual water balance components of streamflow, ET (soil evaporation, transpiration, interception), groundwater storage change, groundwater loss and soil moisture change were then assessed as fractions of precipitation for each hydrological year in the calibration and evaluation period (Section 3.2.3). Total precipitation, averaged over the area of the 31 watersheds, is 900 mm for 2011–2012 and 680 mm for 2012–2013. Total annual precipitation in the evaluation period (2013–2018) ranges from 397 mm to 700 mm.

3. Results and discussion

3.1. Impact of model parameters and parameterization options on model outputs

The baseline simulation results are presented first in Section 3.1.1. The change in the output of WRF-Hydro with Noah-MP (total streamflow, peak flow and total ET) for simulations based on one parameter change at a time in the baseline parameterization (Table 2), relative to the output of the baseline parameterization, are described in the following sections.

3.1.1. Baseline simulation results

The baseline parameterization of the impact analysis (Table 2) simulated the fraction of average total ET to average total precipitation over two watersheds (st16 and st17) equal to 45 % (4 % interception, 12 % soil evaporation, 29 % transpiration) for the two years of calibration. This fraction is much lower than the observed long-term average ET to precipitation fraction of 76 % (17 % interception, 16 % soil evaporation, 43 % transpiration) for the pine forest monitoring site near the outlets of the two watersheds. The underestimation of ET fluxes keeps the soil wetter and thereby affects surface runoff and percolation losses from the soil column to the groundwater.

The streamflow of the 31 watersheds for the two years was largely overestimated with a median percent bias of 54 % in 2011–2012 and 139 % in 2012–2013. This streamflow overestimation was linked to overestimated baseflow, 30 % in 2011–2012 and 80 % in 2012–2013, resulting from soil column percolation losses. The large positive bias in baseflow for the second hydrological year was found to be related to the contribution of water stored in the groundwater bucket and not released during the first year.

3.1.2. Soil, runoff and groundwater parameters

Among the tested parameters, SLOPE and KSAT, followed by SMCMAX, are the most effective in altering the streamflow amount, as seen in Fig. 3. Relative to the baseline parameter set, no percolation (SLOPE = 0), very low hydraulic conductivity (KSAT = 4 mm h^{-1}) and high porosity (SMCMAX = 0.48) lead to reduction of median watershed streamflow up to 25 %, with SLOPE having the largest effect. Maximum percolation rate (SLOPE = 1), very high KSAT (168 mm h^{-1}) and low porosity (SMCMAX = 0.34) lead to an increase in median streamflow of similar magnitude. These parameters have a direct impact on soil moisture, which in turn affects the available soil water for transpiration. For this reason, the change in median ET has an opposite sign and an almost similar magnitude with the relative change of streamflow. Within the range of possible values of KSAT, the median relative change in total ET is from about −20 % up to + 10 %, which is higher than the change resulting from any of the other soil and runoff parameters.

The same parameters with the addition of REFKDT affect the peak flows most strongly. For REFKDT, the relative change in streamflow (1–1.25) is smaller than the relative change in peak flow (0.6–2.4). The reason for this difference is because REFKDT impacts mainly peak flows, due to its regulation of the infiltration rate. The effectiveness of REFKDT in infiltration increases with drier soil moisture conditions, as seen in the comparison of the relative change in peak flow for the two years in Fig. 3 and with increasing precipitation rate. For these reasons, previous studies (e.g., Yucel et al., 2015; Zhang et al., 2020), which focused on short-term extreme events found a strong regulation of REFKDT in simulated streamflow. Regarding other parameters, the low values of SLOPE (0), and KSAT (4 mm h^{-1}) result in opposite signs of the relative

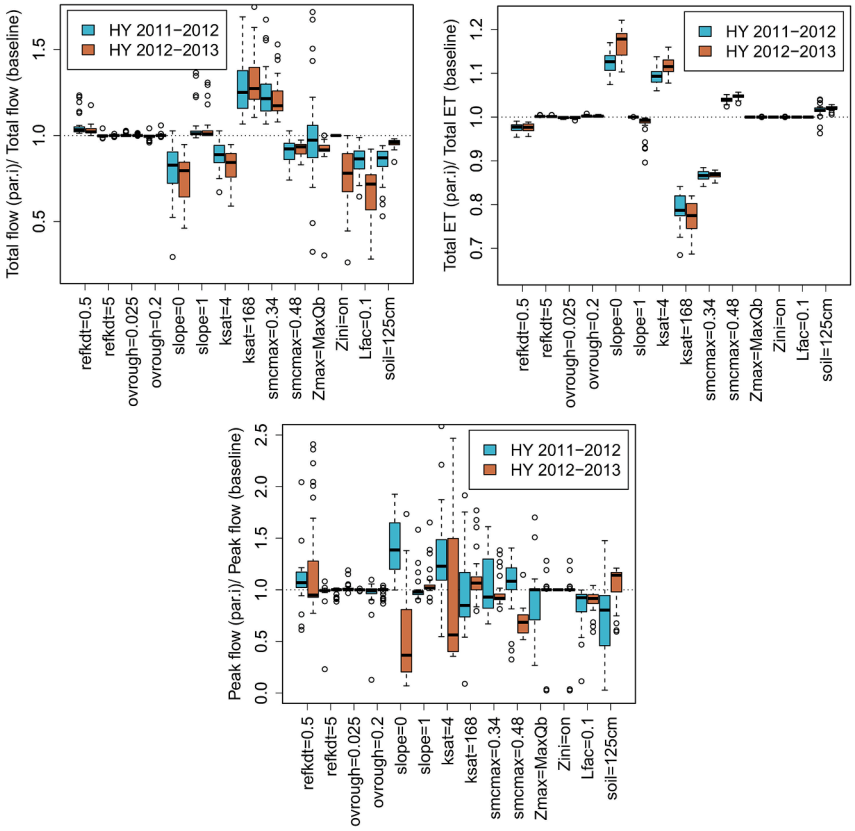

Fig. 3. Boxplots of the change of modeled streamflow (top left), evapotranspiration (ET) (top right) and peak flow (bottom), relative to a baseline scenario, of 31 watersheds, resulting from changes in soil, runoff and groundwater bucket model parameters (x-axis), for hydrological years 2011–2012 and 2012–2013. The description of the parameters can be found in Table 2.

change of peak flow in the two hydrological years. These specific parameter values lead also to the highest ET increase in both years. The decrease of peak flow with no percolation (SLOPE = 0), for instance, in the second hydrologic year, may be linked to the enhanced transpiration that reduces the soil moisture, impeding the increase in peak flow due to saturation excess. In 2011–2012, peak flows are instead enhanced with no percolation (SLOPE = 0), probably because of saturation excess in the very wet conditions.

The effect of the GW loss factor (L_{fac} = 0.1) is a reduction of total streamflow up to 30 % in the wet year and in the second drier hydrological year by 15 % to 75 % for the different watersheds. A comparable reduction is achieved with Z_{ini} in the second hydrological year because the water depth in the bucket was set to 0 for the 28 ephemeral watersheds and to 0.1 times the water depth in the bucket for the continuous flow watersheds (st12, st13, st14) at the beginning of the second year (October 2012). Both parameters are useful for the reduction of the substantial positive streamflow bias of the baseline parameterization. However, L_{fac} induces groundwater losses and thus reduced baseflow throughout the simulation period. Z_{ini} creates, instead, a reduction in baseflow with a discontinuity in the baseflow component of the hydrograph at the time of initialization. Setting the parameter ZMAX equal to the maximum long-term annual baseflow per watershed has a heterogeneous effect on the total streamflow of the 31 watersheds, in contrast to the homogeneous response resulting from changes in the soil parameters. Total streamflow is reduced in some watersheds and increased in some others up to ±25 % in the wetter 2011–2012, and less in 2012–2013. This variable impact of ZMAX on total streamflow among watersheds justifies the manual calibration of ZMAX per watershed, as described in Section 2.5.

Considering the high variability of the model outputs to the percolation parameter SLOPE, it was selected to be a calibration parameter. Among the two soil properties KSAT and SMCMAX, the KSAT was selected to be calibrated because of its larger impact and variability among watersheds, compared to SMCMAX. The soil depth for the calibration runs was set to 125 cm, because it reduced the streamflow amounts that were overestimated by the 100 cm soil depth of the baseline parameterization. Further, parameter REFKDT, which impacts the magnitude of peak flows, was selected for calibration.

3.1.3. Vegetation parameters

The magnitude of the relative change of total streamflow and ET resulting from the representation of vegetation density (GVF and LAI) is almost the same as the magnitude of the relative change due to the selection of the stomatal conductance model, i.e., the Jarvis model (Fig. 4). The option for monthly GVF (DVEG = 1) results in a median reduction in ET by 15 % up to 25 % relative to the yearly maximum GVF (DVEG = 4, baseline run). The computation of GVF as a function of the prescribed monthly LAI (DVEG = 3; Eq. (7)) results in higher GVF values and 20 % higher ET than both the monthly prescribed GVF (DVEG = 1) and yearly prescribed GVF (DVEG = 4; baseline). The replacement of prescribed LAI values with satellite-derived values for different land use categories and GVF equal to 1 (LAI = Copernicus) has a small impact on streamflow and ET, which are reduced and increased up to 5 %, respectively.

The Jarvis stomatal conductance model increases the total annual ET by 15 % – 20 % compared to the ET obtained by the default option of Ball-Berry model. The refinement to the Jarvis model, with the inclusion of the description of nocturnal transpiration, increases ET, on average, with an additional 10 %–15 %. The adjustment of the parameter controlling the interception of precipitation by canopy (CH2OP) to a value equal to 0.5 mm per unit LAI instead of the prescribed 0.1 mm leads to a

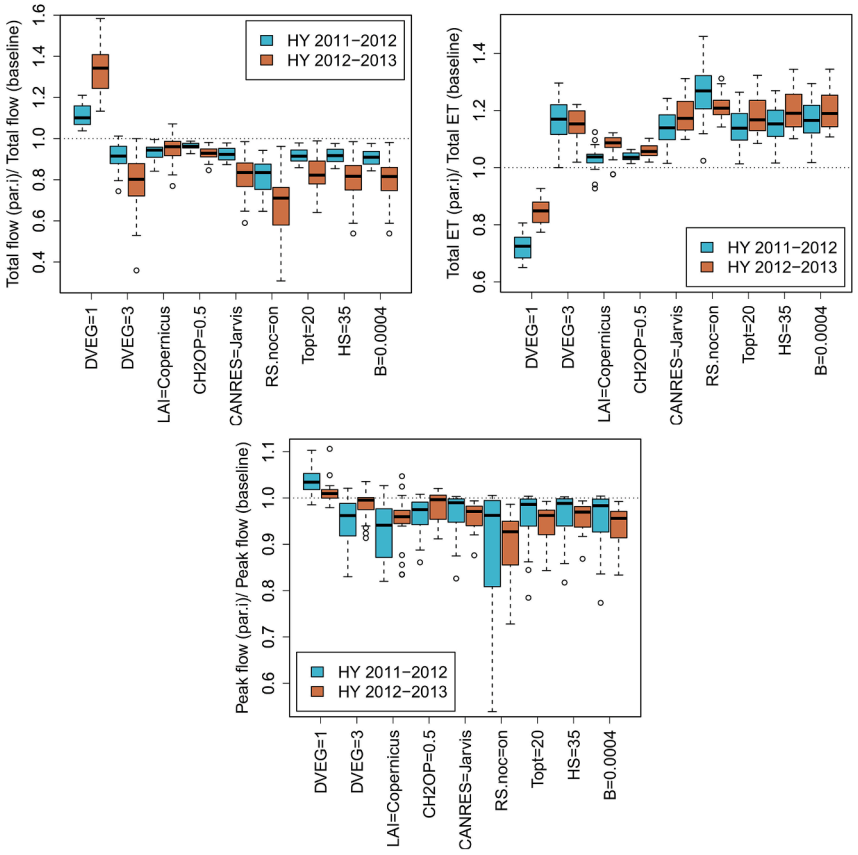

Fig. 4. Boxplots of the relative change of modeled streamflow (top left), evapotranspiration (ET) (top right) and peak flow (bottom) to changes in vegetation model parameters (x-axis), relative to a baseline scenario for hydrological years 2011–2012 and 2012–2013. The description of the parameters can be found in Table 2.

Table 3
The WRF-Hydro distributed parameter names, watershed characteristics, area covered per characteristic, parameter estimation range and the PEST calibrated parameter values.

Parameter	Unit	Watershed characteristic		Area (%)	Min value	Max value	Calibrated value
Land surface classes	1	Coniferous forest	slope < 5 %	9	3.0	6.0	6.0
REFKDT (-)	2		5 % <= slope < 10 %	23	2.5	5.0	3.9
	3		slope >= 10 %	14	1.5	4.0	1.6
	4	Shrubland	slope < 5 %	7	3.0	5.5	5.5
	5		5 % <= slope < 10 %	11	2.0	4.5	2.2
	6		slope >= 10 %	6	1.0	4.0	3.4
	7	Agricultural land	slope < 5 %	16	1.0	4.0	4.0
	8		5 % <= slope < 10 %	12	0.5	3.5	3.5
	9		slope >= 10 %	2	0.2	3.0	0.2
Geology classes	1	Vulcanic Complex		12	0.1	1	0.24
SLOPE (-)	2	Ultramafic Complex		10	0.1	1	0.56
	3	Basal Group, Diabase		46	0.1	1	0.87
	4	Gabbro, Plagiogranite		9	0.1	1	0.96
	5	Sedimentary		23	0.1	1	1.00
Soil classes	1	Vulcanic Complex	Clay loam	12	5	20	13
KSAT (mm h^{-1})	2	Ultramafic Complex	Sandy loam	10	10	70	42
	3	Basal Group, Diabase	Loam	46	5	20	12
	4	Gabbro, Plagiogranite	Loamy sand	9	30	70	56
	5	Sedimentary	Clay loam	23	5	20	10

small increase in ET, due to increased intercepted precipitation. The three parameters TOPT, B and HS in the Jarvis model stress functions have almost no impact, giving the same results as the baseline parameter set.

The total ET increase by 15 % up to 20 % with the Jarvis model, relative to the Ball-Berry, was found to be closer to the values of local ET observations (Eliades et al., 2018b). This underestimation of ET by Ball-Berry in this semi-arid Mediterranean environment agrees with the results reported by Zheng et al. (2019) for the suitability of Jarvis in semi-arid regions of the conterminous United States. For these reasons, the Jarvis model, with the formula for nocturnal transpiration replaced the Ball-Berry model in the model code of this study. The Jarvis model parameter TOPT was set to 20℃, despite its negligible impact, because the specific value is suggested for Mediterranean vegetation by Larcher (1995) and for crops by Wang et al. (2017). For a more realistic representation of GVF and LAI, the remote-sensed Copernicus-based LAI was used for the calibration model runs of this study.

The Jarvis stomatal conductance enhanced with the nocturnal component leads to increased ET relative to the baseline Ball-Berry (30 %), which corresponds to a similar reduction in soil moisture. The groundwater loss function continuously reduces the groundwater storage in the bucket as a function of the groundwater level and this induces reductions in baseflow overall, but also reduction of large baseflow releases during peak flow events. Thus, a new baseline parameterization, based on modified Jarvis and groundwater bucket equations, could possibly lead to an altered impact of the tested parameters. The difference in the parameter impact under drier conditions in soil and groundwater can be understood by comparing the relative changes of streamflow, peak flow and ET in the two hydrological years used in this study. These relative changes are mostly similar in both the very wet 2011–2012 and in the less wet 2012–2013, particularly for the total streamflow and total ET. The significance of these findings is also indicated by comparing the relative impact of the same parameters and parameterizations for the 31 watersheds. Parameters SLOPE, KSAT and L_{fac} as well as most of the vegetation parameters result in similar relative changes in streamflow and ET, in both years as seen in Fig. 3 and Fig. 4 as well as when each watershed is examined individually. For instance, for st1 and SLOPE equal to zero, the relative changes in streamflow (0.92 in 2011–2012 and 0.87 in 2012–2013) and in ET (1.09 in 2011–2012 and 1.14 in 2012–2013) have similar magnitude. The same patterns can also be observed for KSAT and L_{fac} and most vegetation parameters and for other watersheds.

The results of this study show that the baseline parameterization of WRF-Hydro and particularly of Noah-MP, from the parameterizations of which the soil, runoff and vegetation parameters originate, exhibit strong biases in ET fluxes in the semi-arid environment of the study area. These findings are indicative of potentially strongly biased fluxes to the atmosphere, which may affect the modeling of atmospheric variables, such as in the WRF atmospheric model, which can be coupled to Noah-MP and to WRF-Hydro, as pointed out by Lin and Cheng (2016). In addition, through the impact analysis it was seen that soil and vegetation parameters and the GW bucket maximum depth ZMAX, as well as both the new GW loss factor and the adjustment in Jarvis model equation are necessary to reduce the streamflow overestimation. The largest reductions, on average for all watersheds, were up to 25 % for SLOPE, KSAT and the adjusted Jarvis equation. Cuntz et al. (2016) reached similar conclusions about the sensitivities of soil and vegetation parameters in a global sensitivity analysis for water balance components simulated with Noah-MP for locations in the eastern United States. The influence of soil and runoff parameters on simulated surface fluxes with Noah-MP was also highlighted by Li et al. (2020).

3.2. Model calibration and evaluation

3.2.1. Calibration of distributed and groundwater parameters

The distributed model parameter calibrated values for REFKDT, SLOPE and KSAT for the different land surface and geology classes are presented in Table 3 and Fig. 2. The calibration of the 19 parameters values was completed after nine PEST iterations with 198 WRF-Hydro model runs. The computational cost was 260 CPU hours per WRF-Hydro run for two years of simulations. The manually calibrated value of ZMAX ranged between the long-term annual average and maximum total baseflow for 17 watersheds. For 12 watersheds, ZMAX was set below the long-term average baseflow and for two watersheds, ZMAX was set above the long-term maximum baseflow.

Overall, the grid-based calibration of distributed model parameters resulted in calibrated parameter values, generally, within the calibration range and consistent with the expected hydrological function of watershed characteristics. For instance, the REFKDT values were the highest and lowest for the topographic slope lower than 5 % and larger than 10 %, respectively, for the three land use classes. From Table 3, it is also seen that some calibrated REFKDT values are equal to the maximum or minimum value of the range set for the calibration. The calibrated values are most often close to the maximum values for the land surface classes with slope<5 %. Low topographic slope is expected to increase infiltration, which is simulated with high REFKDT values. These calibration results indicate the high infiltration rates, which were correctly assigned by PEST, through the REFKDT values for flat or nearly flat areas.

Increasing the value of REFKDT above these maxima reached during calibration, will only induce, however, minor difference in the simulated streamflow, according to Camera et al. (2020). These authors tested REFKDT values ranging from 0.3 up to 1000 and showed that the REFKDT impact on streamflow is well captured with values up to about five, and only small variations in total discharge could be observed with REFKDT up to about 100.

For parameter SLOPE, the gridded areas with sedimentary, gabbro or diabase geologies were assigned values higher than 0.85. This result is consistent with the high bedrock permeability of these formations (Udluft et al., 2006). Parameter SLOPE values close to one lead to maximum percolation rate. The calibrated values of KSAT (ranging from 2.8×10^{-6} and 1.6×10^{-5} m s^{-1}) are also representative of the soils of Troodos. The highest hydraulic conductivities were assigned to soil classes of sandy loam and loamy sand, which correspond to the geological classes of the uppermost part of Troodos (gabbro, plagiogranite and ultramafic complex). The spatial calibration has also resulted in higher value of KSAT for the soil class of clay loam than that of loam, despite that clay containing soils are expected to have a lower KSAT than loam, for instance. These results are indicative of the high uncertainty of soil texture over Troodos, as reported by Camera et al. (2017).

The grid-based calibration for streamflow can be considered a useful method to estimate spatial values of soil properties that have not been measured. The advantage, in addition, of the grid-based calibration at multiple watersheds, based on watershed characteristics, is that the calibrated distributed parameters can be used for ungauged streams. One limitation is that GW bucket parameters could not be linked to watershed characteristics in this study. For ungauged basins, GW parameters could instead be estimated from extrapolation of GW parameters of neighboring watersheds. Nevertheless, the limitation of GW parameters, is only relevant for streamflow and not for any land surface processes, which control ET.

3.2.2. Calibration and evaluation results

The evaluation results of the model configuration based on the grid-based calibration of distributed parameters, are shown in Fig. 5. Positive NSE and KGE values were obtained for 28 out of 31 watersheds, with median NSE equal to 0.49 in the calibration period. The model efficiency in the evaluation period (2013–2018) is lower, with a median NSE of 0.02 and positive NSE and KGE in 16 and 21 watersheds, respectively. The number of watersheds with full streamflow observation time series in the evaluation period was, however, also lower (31 watersheds in 2013–2014 and in 2014–2015, 26 in 2015–2016, 20 in 2016–2017 and 15 in 2017–2018). Despite this uneven number of watersheds in each hydrological year, a positive correlation of NSE and KGE with total precipitation per hydrological year (total precipitation shown in Fig. 8), with increasing efficiency metrics for increasing precipitation, was observed considering all watersheds, but also only considering the 15 watersheds with full records during the evaluation period. The median NSE and KGE for the entire period were 0.24 and 0.55, with positive metrics for 28 and 29 watersheds, respectively.

The mean absolute error (MAE) in the volume of streamflow is, on average, <0.5 mm per day in both the calibration and evaluation period, and the MAE in the evaluation period is larger than the MAE in the calibration period only in one (2014–2015) out of the five evaluation years. The relative bias of total streamflow per hydrological year is less than ±25 % for 26 watersheds for the calibration period, which is a substantial improvement relative to the bias of 50 % – 100 % in the

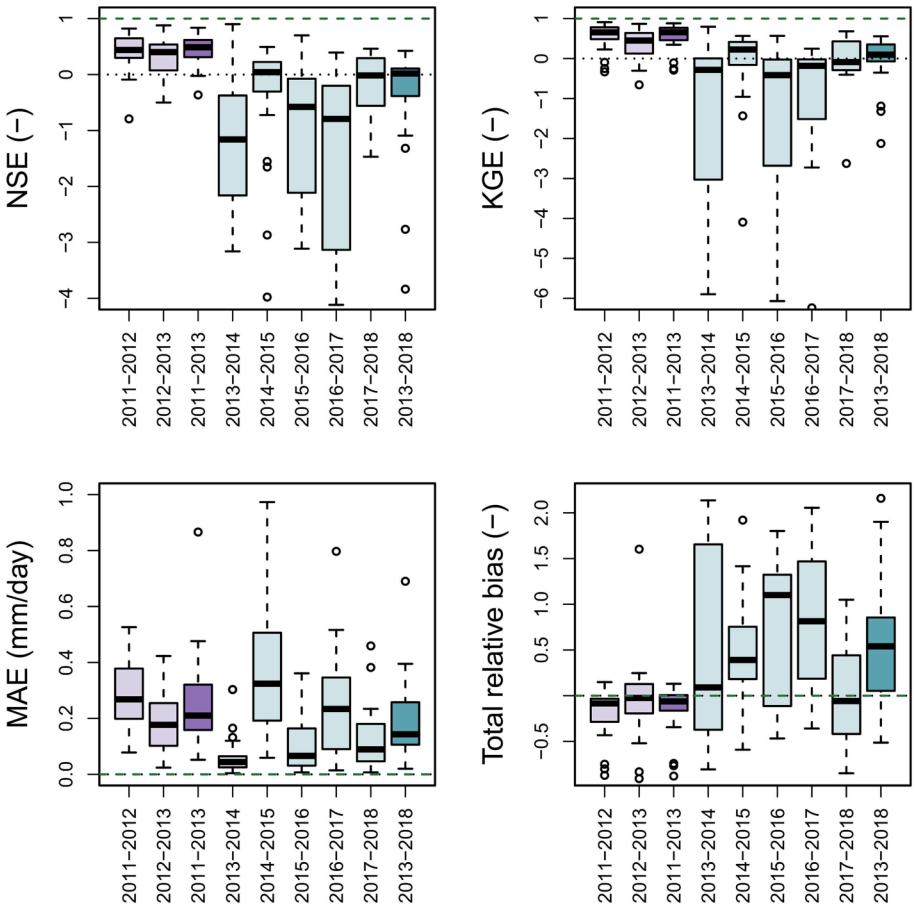

Fig. 5. Boxplots of the 31 watersheds for the Nash-Sutcliff efficiency (NSE), Kling-Gupta efficiency (KGE), mean absolute error (MAE) and relative bias, with each box representing the variability of the values of each metric for the 31 watersheds for each hydrologic year in the calibration and the evaluation period.

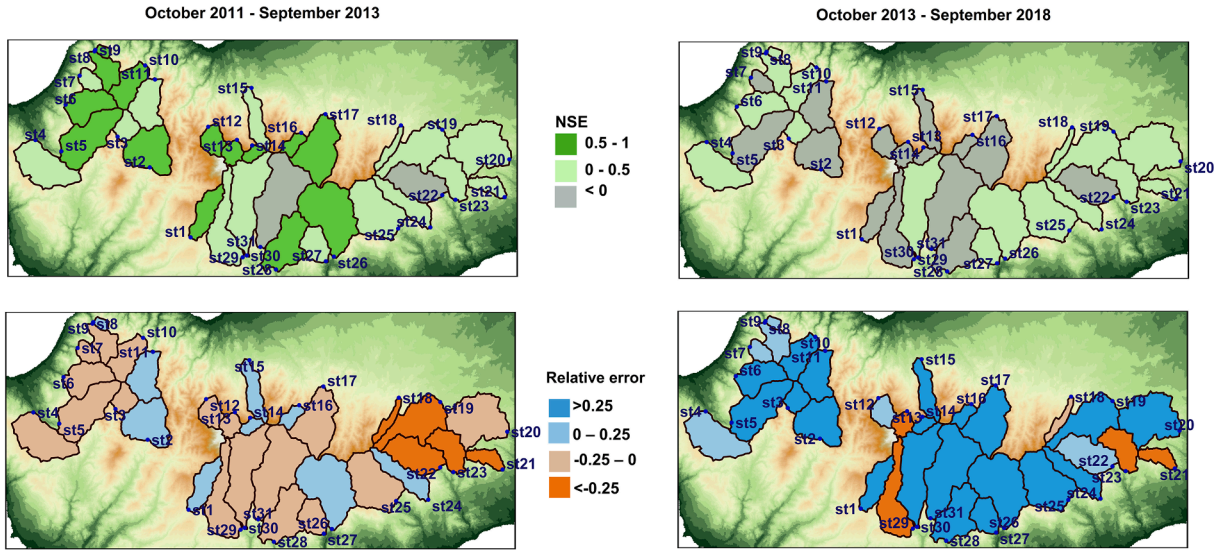

Fig. 6. Maps of the 31 watersheds with the area of each watershed colored according to the Nash-Sutcliff efficiency (NSE; top) and Relative error (bottom) achieved by WRF-Hydro for the calibration period (left) and the evaluation period (right).

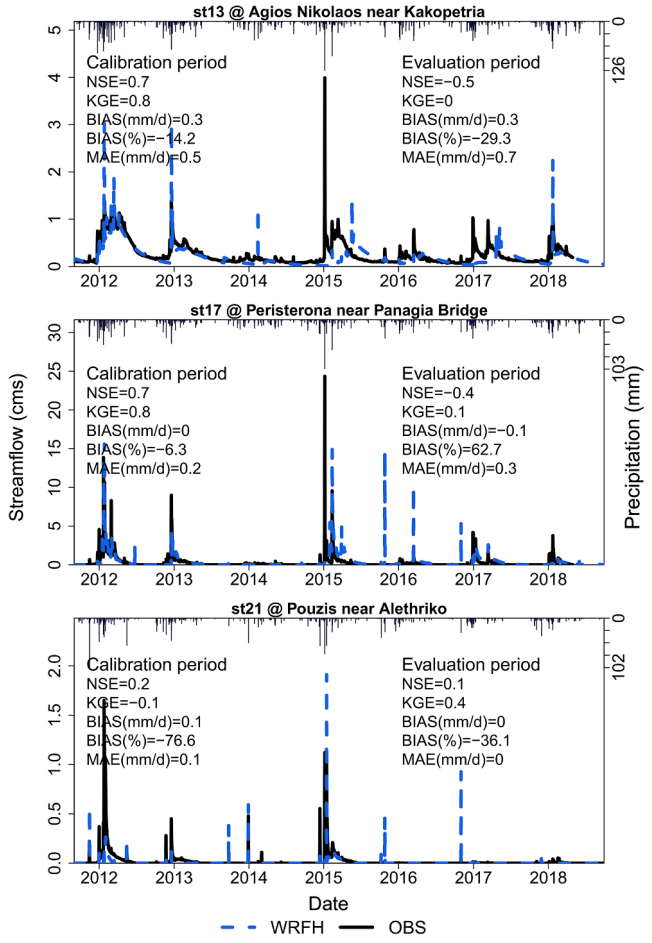

Fig. 7. Hydrographs of WRF-Hydro simulated streamflow and observed streamflow (m^3s^{-1}) at three watersheds with evaluation metrics for the calibration period (2011–2013) and the evaluation period (2013–2018).

same period with the baseline parameterization. An exception is the group of five watersheds on the eastern flank of Troodos mountains (Fig. 6), which receives less rainfall than the west and central part of the mountains. A large overestimation of total streamflow is evident from Fig. 5 and Fig. 6 for the evaluation period, particularly for the three driest hydrological years (2013–2014, 2015–2017).

The examination of the simulated and observed hydrographs in Fig. 7 for three watersheds of different prevailing hydrological conditions, i.e., non-ephemeral (st13) and ephemeral (st17 and st21) confirms the results of Fig. 5. The hydrographs of all 31 watersheds are presented in Appendix C. The modeled streamflow follows very well the observed streamflow in the calibration period for most watersheds. The most profound errors in the evaluation period are linked to baseflow and the mismatch between observed and simulated flow during the rising and descending limb of the hydrographs in the wetter years. The timing of simulated peak flows agrees with the observed peak flows despite some errors in the magnitude of peak flows, especially in days with high accumulated precipitation, about 50 mm and above. For the wettest hydrological year of the evaluation period (2014–2015), the first simulated peak flow is delayed for many watersheds, relative to observations. This delayed peak flow could be attributed to differences in the growth of the forest understory and the stream network vegetation, which are represented by time-invariant roughness coefficients in the model.

The errors in peak flows in days with high accumulated precipitation could be linked to errors in the precipitation because the rain gauge network that was used for the generation of the gridded forcing data may not sufficiently capture the spatial variability of the rainfall over the mountains (Sofokleous et al., 2021). This explanation is even more important in small watersheds. The small size of watersheds implies potentially large streamflow volume errors, in case of errors of the spatially interpolated precipitation. Short concentration times in combination with the uncertainty of precipitation may also lead to errors in the timing of peak flows.

The reduction of performance in the evaluation period is common for WRF-Hydro, as seen in other studies as well. For a 3-year simulation period and a 1281 km^2-sized basin in S. Italy, Senatore et al. (2015) reported a reduction in NSE from about 0.9 to about 0.3, moving from the calibration to the evaluation period. These authors attributed the NSE reduction to the peak flows underestimation, which was related to the limitations in simulating the intensity and duration of precipitation. For simulation of two extreme precipitation events for 22 watersheds in the Troodos mountains, Camera et al. (2020) reported NSE and KGE values above 0.5 for most watersheds for the calibration event and a reduction of the values of the two efficiency metrics, remaining mostly

positive, for the evaluation event, similar to this study. They attributed the performance reduction to overestimation of peak flows, which could have been lower with increased roughness coefficients.

Biases in the baseflow component of the hydrographs, as described above, could be partly explained by the findings of previous studies for the groundwater processes in Troodos. Boronina et al. (2003) used the 2D groundwater MODFLOW code to model groundwater processes of three Troodos watersheds (st29, st30, st31) and found substantial groundwater exploitation. Christofi et al. (2020) showed, with integrated observations and modeling, that groundwater flows across subwatersheds. The main reason for the latter is that in the complex, fractured Troodos aquifer system, hydrogeological (subsurface) basins have a different extent than hydrologic (surface) watersheds. The findings of Boronina et al. (2003) and Christofi et al. (2020) are indicative of groundwater losses, simulated by WRF-Hydro here with the new GW loss factor. Rummler et al. (2022) found that the implementation of a different groundwater parameterization, i.e., a 2D groundwater table scheme, with soil moisture and groundwater interaction, improved WRF-Hydro streamflow simulations in the upper Danube river basin. However, considering that modeling groundwater in fractured aquifers, such as those in Troodos, is subject to large uncertainties, the calibrated GW bucket model of WRF-Hydro with the groundwater loss factor introduced in this study is a useful conceptualization of complex groundwater processes. Such processes are groundwater losses beyond the watershed boundaries and water use abstractions that cannot be observed or modelled individually.

The low final NSE calculated for the evaluation of WRF-Hydro, can be due to the relatively large number of watersheds (31) calibrated simultaneously for a relatively small number of parameters (19). The consideration of alternative or additional soil parameters to be calibrated, e.g. porosity and the exponent in the shape parameter for soil resistance, as suggested to be very sensitive parameters by Cuntz et al. (2016), could have provided further performance improvements with the grid-based calibration. Yet, the assignment of distributed values to further soil properties would require additional computational resources and data for the spatial distribution of these properties, which is currently lacking. Furthermore, the equifinality of the results, i.e., similar relative change of total streamflow, ET and peak flow in two different hydrological years, with changes in the values of different parameters, as discussed in Section 3.1.2 and Section 3.1.3, is another limiting factor for adding more parameters in the calibration parameter set. An improved WRF-Hydro performance could possibly also be achieved with a variable soil depth across the simulation domain, as Fersch et al. (2020) proposed, which is however unsupported in the latest WRF-Hydro version (v5.2).

The degradation of the model performance in this study could have been lower in the evaluation period, if a longer calibration period with an additional year of different precipitation conditions would have been included. There are, however, certain considerations, which imply that the poor model performance in dry years is not just subject to the selected period of calibration. WRF-Hydro is a physically-based model and the calibration of parameters used in the physically-based model equations for two years, with interchanging very wet, wet and dry periods exposed the calibrated parameters to all of these conditions. The aforementioned exploitation of groundwater resources over Troodos, not included in the WRF-Hydro code, could be enhanced in drier years and this will have a direct impact on baseflow. This study tested, in addition to the loss factor, the initialization of the groundwater bucket at the beginning of each hydrological year, as a method to resolve the overestimation of baseflow in simulations of consecutive hydrological years. This example highlights how water resources exploitation is not part of the physically-based processes of WRF-Hydro and that the groundwater bucket level has to be manually adjusted to account for local water use.

The low performance of semi-arid watersheds with ephemeral streams can also be explained by the changing vegetation properties in the stream network. Wet conditions in one year promote the development of riparian vegetation within the streams during the low flow season. These changed stream roughness conditions remain in following dry years and hinder flow reaching the watershed outlet. Part of this flow becomes ponded water, which eventually becomes ET. The stream roughness will decrease when the vegetation flattens during high precipitation and high flow events. Adding dynamic functions for some parameters to account for temporal variation of land surface and channel properties (e.g. REFKDT, overland and channel roughness) could alter the response of watersheds, particularly for dry years and ephemeral streams. The spatial calibration of these time-variant parameters could in this case be performed for land surface classes based on high resolution satellite-derived LAI.

This study showed that the performance of small semi-arid watersheds exhibits high relative change to model soil and vegetation parameters as well as to the total precipitation in the year of simulation. The water-limited environment of semi-arid areas requires improved parameterizations reproducing ET in Noah-MP, which is the dominant water balance component for the largest part of a hydrological year. At the same time, the wet winter period of the year coincides with the period when the radiation is relatively low and thus, the soil moisture and runoff parameterizations are important for simulating surface and subsurface runoff and percolation to the groundwater. For streamflow simulations for entire hydrological years, such as for seasonal streamflow forecasting, the baseflow parameterization becomes important, because baseflow is the dominant component in the hydrograph. For the latter, the soil physics parameterization and parameters SLOPE and KSAT, which control the inflow into the groundwater bucket are important. For the bucket outflow, the size of groundwater bucket (ZMAX) and groundwater bucket outflow coefficients are other model components that should be considered in the calibration of the model.

3.2.3. Water balance evaluation

The simulated watershed area-average water balance components of the 31 watersheds are shown in Fig. 8. The partitioning of precipitation into the water balance components of soil evaporation, canopy intercepted and evaporated water, canopy transpiration, runoff, soil moisture change, groundwater storage change, groundwater loss and dam storage change (the last not shown), in each hydrological year, is dominated by the losses to the atmosphere. Transpiration accounts for about 40 % of the total water balance, on average, for all watersheds. In addition, soil evaporation and intercepted water have an average contribution to the total water balance of about 30 % and 15 %, respectively. Therefore, ET returns about 85 % of the input precipitation to the atmosphere. The next most dominant component of the water balance is the total runoff, with an average contribution of 15 %. A smaller contribution in the water balance, less than $\pm$10 %, is due to the change in the soil and groundwater storage, and to a much lesser extent to losses from the groundwater and dam storage. Soil and groundwater storage changes show positive changes in the wettest years, such as 2011–2012 and 2014–2015. With these results, the positive impact of the groundwater bucket in WRF-Hydro and the GW loss factor introduced here for streamflow simulations in semi-arid environments can be seen once more. The largely overestimated streamflow by the baseline WRF-Hydro, as shown in this study, can be reduced, in order to better match the ephemeral behavior of semi-arid streams with the adjustment of storage capacity of the GW bucket and the use of the GW loss factor. The average water balance closure error was calculated to range within $\pm$5 %. Possible sources for this figure could be the error in the numerical solution of the soil water flow in WRF-Hydro code (maximum water balance error allowed per time step = $\pm$0.1 mm) and the mismatch between the watershed area of Noah-MP and WRF-Hydro from both of which the water balance components were extracted. The watershed border in Noah-MP is based on its 1-km grid resolution whereas the watershed border in WRF-Hydro was delineated on the 100-m grid.

The temporal variability of these water balance components seems to

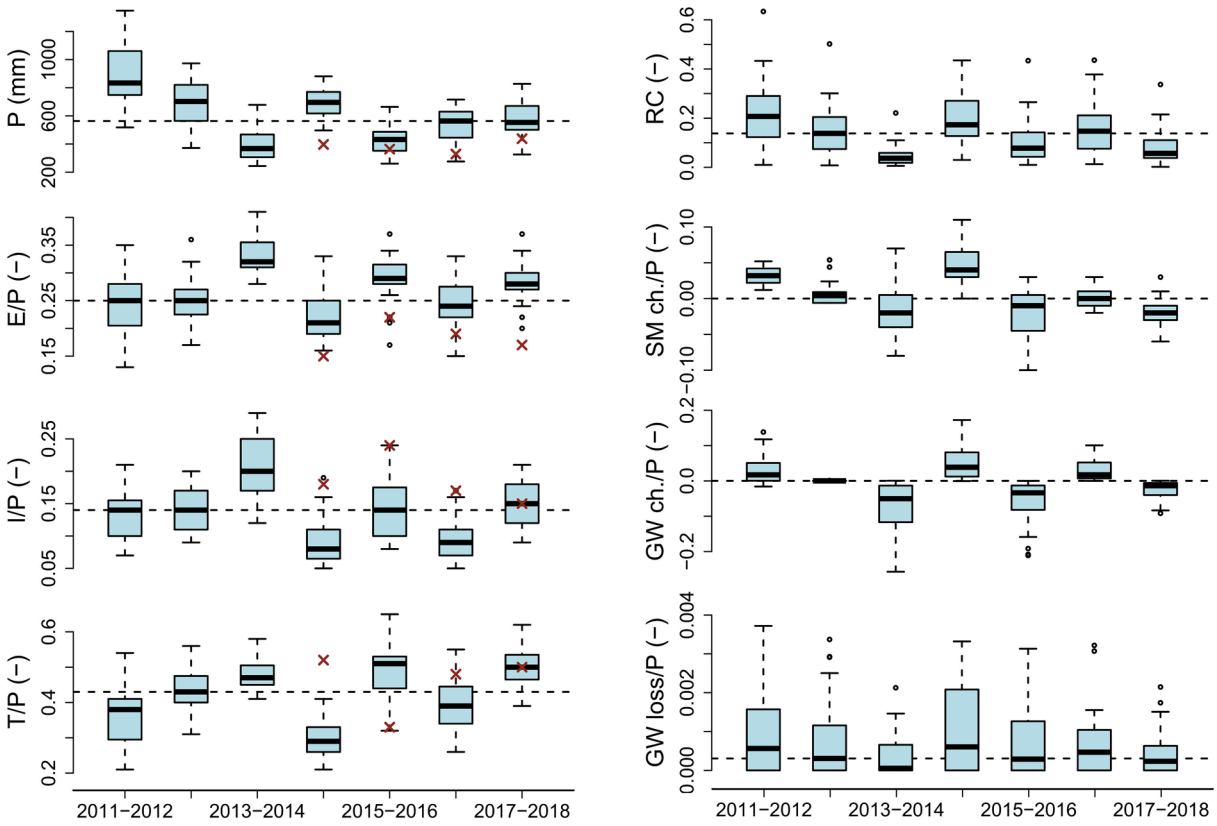

Fig. 8. Boxplots, as in Fig. 3, of the total precipitation (P) and the ratios of the modeled soil evaporation (E), canopy interception (I), transpiration (T), soil moisture change (SM ch.), groundwater storage change (GW ch.) and groundwater loss (GW loss) to precipitation and the modeled runoff coefficients (RC) for 31 watersheds and seven hydrological years. Crosses represent annual average observed values at the pine forest monitoring site.

be correlated with the total precipitation. For instance, the highest and lowest watershed average runoff coefficients are observed in the wettest (2011–2012) and driest (2013–2014) years, respectively. The water storage changes in soil and groundwater bucket, relative to the total precipitation, follow the change in total precipitation from year to year and the magnitude of the change is more evident in the transition between years when one of them is either very wet or very dry. For instance, the dry hydrologic year 2013–2014 after the wet 2012–2013, with total precipitation 400 mm and 680 mm, respectively, has a soil and groundwater storage change equal to −2% and −6%, on average, for all watersheds. The ratio of evaporation, interception and transpiration to the total precipitation seems to be inversely correlated with the total precipitation. During the driest years, the dominance of the three components is higher than in the wetter years. Taking into account,

Table 4
Total transpiration (sum) and percent bias (PBIAS) for the period January 2015 to December 2017 separated in amounts occurred during day and during night from observations at the monitoring site of Eliades et al. (2018a) and model results with the Jarvis model and the improved Jarvis model with nocturnal transpiration at the corresponding model grid cell.

	Sum (mm)	PBIAS (%)
Day		
Observations	418	
Noah-MP Jarvis	239	−43
Noah-MP Jarvis nocturnal	443	6
Night		
Observations	94	
Noah-MP Jarvis	27	−71
Noah-MP Jarvis nocturnal	122	30

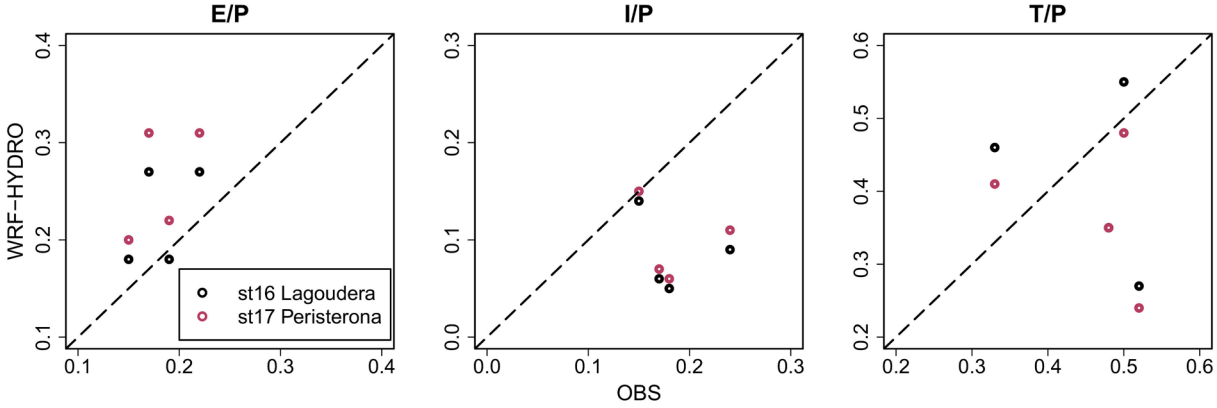

Fig. 9. Scatterplots of the observed and watershed average simulated fractions of evaporation to precipitation (E/P), interception to precipitation (I/P) and transpiration to precipitation (T/P) for the hydrological years from 2014 to 2018.

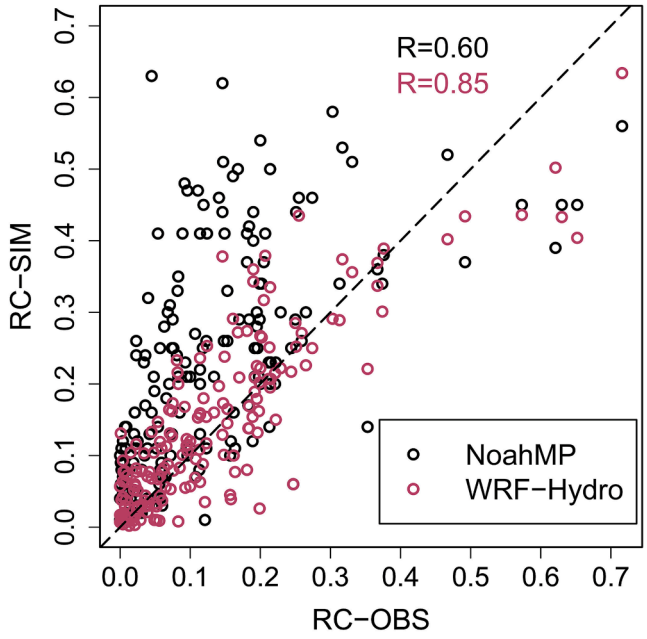

Fig. 10. Scatterplot of the runoff coefficients of 31 watersheds per hydrological year for seven years for observed data (RC-OBS) against simulated data (RC-SIM) and the correlation coefficient R with Noah-MP and WRF-Hydro models.

however, the amount of precipitation per hydrologic year, the total amount of evaporated and transpired water is higher during the wet years.

The temporal pattern of the water balance components modeled by WRF-Hydro seems to generally follow observations at the pine forest monitoring site of Eliades et al. (2018a) (Fig. 8), which is located close to the boundary of Peristerona watershed (st17) and just downstream of the Lagoudera watershed (st16). The precipitation at the site is in the driest 25 % percentile of the long-term average precipitation of the 31 watersheds (Fig. 8). The four-year average (2014–2018) observed ratio of evaporation to precipitation (E/P) was 0.18, whereas the simulated E/P was 0.23 for Peristerona and 0.26 for Lagoudera. The total observed interception to precipitation ratio (I/P), according to long-term interception observations by Eliades et al. (2022) was 0.19, and the modeled I/P was 0.09 for Peristerona and 0.10 for Lagoudera. The lower vegetation density for coniferous forest in the model (Copernicus LAI = 1.3; Table B1, Appendix B) compared to that observed at the monitoring site (LAI = 2.38) can explain the lower simulated interception rates and higher simulated soil evaporation (Fig. 9). The four-year average ratio of transpiration to precipitation (T/P) at the site, about 0.45, is very close to the average ratio simulated for the Peristerona watershed (0.42) and for the Lagoudera watershed (0.37) for the same years. The partitioning of observed and modeled transpiration to day-time and nocturnal amounts (Table 4) for the years 2015 to 2017 shows that the improved Jarvis model reduces the total period transpiration bias for the location of the monitoring site for both day and night time to 25 and 28 mm respectively. Despite the improvement in the simulated amounts, the Jarvis model and the the parameters of the nocturnal Jarvis radiation equation should be further tuned to match the diurnal transpiration patterns too. Overall, the partitioning of the three water balance components to precipitation is simulated with a maximum difference of 10 % of total precipitation relative to observations.

Zheng et al. (2019) found that for the improvement of annual and seasonal modeling of ET through model simulations with Noah-MP, the impact of terrestrial water and of vegetation changes during the vegetation growing season needs to be considered. To account for the vegetation changes, Arsenault et al. (2018) suggested the Ball-Berry stomatal conductance model, which is able to simulate dynamic vegetation changes, which however underestimates observed ET relative to the Jarvis model as seen for the semi-arid environment of this study, as well as in Ingwersen et al. (2015) and Zheng et al. (2019). For these reasons, including the seasonal variation of LAI at high spatial resolution, as well as the improvement of Jarvis model for accounting for the local ecohydrological processes, as suggested in this study, particularly during the growing season need to be considered for the simulation of the magnitude and temporal variability of the ET components.

The impact of lateral routing, which is enabled in WRF-Hydro, unlike the stand-alone Noah-MP LSM can be seen in Fig. 10. The WRF-Hydro runoff coefficients are closer to the 1:1 line with the observed runoff coefficients compared to the Noah-MP runoff coefficients. The correlation coefficient of WRF-Hydro runoff coefficient against observed values was 0.85, compared to 0.60 for the Noah-MP runoff coefficients. In addition, the average WRF-Hydro runoff coefficient was 0.13, very close to the observed average of 0.14, whereas the average value obtained with Noah-MP was 0.22. The reduced WRF-Hydro runoff amounts are related to the process of lateral routing and re-infiltration of routed surface water. Zhang et al. (2020) found that the re-infiltration ratio and runoff coefficient in WRF-Hydro are two correlated indices. Furthermore, WRF-Hydro here is enhanced with the loss factor introduced in the GW bucket model (Section 2.2.1) that contributes to groundwater losses and thus reduced baseflow. WRF-Hydro has in some cases, however, higher runoff coefficients than Noah-MP. This is because there might be a baseflow contribution to the total WRF-Hydro streamflow from groundwater stored in the bucket in the previous year. Overall, these results clearly indicate the added value of using WRF-Hydro for water balance investigations.

4. Conclusions

In this study, a grid-based approach was tested to calibrate the spatially distributed parameters of the WRF-Hydro model using the PEST software. The model equations of the groundwater bucket module and of the Jarvis stomatal conductance model were improved to describe groundwater losses and nocturnal transpiration. An impact analysis of different parameters, parameterization options and the improved equations on total streamflow, total evapotranspiration (ET) and peak flows of 31 Mediterranean mountain watersheds, in a two-year period, was performed. The parameter impact was examined relative to a baseline WRF-Hydro configuration. For the baseline parameter set, the parameters for runoff, soil texture and soil depth were adjusted, relative to the default WRF-Hydro and Noah-MP parameterization, to represent local conditions. The median bias of streamflow in the baseline parameterization was 54 % and 139 %, respectively, in two years of calibration. The final model configuration was based on the results of the impact analysis and of the grid-based calibration in the two-year period, and was evaluated in a five-year period. The main findings of this study are:

- Within the range of change of the soil parameter values or vegetation parameterization options, the median streamflow and ET of the 31 watersheds could be increased or decreased up to about 30 %, relative to the baseline model parameterization. The largest impact in total streamflow, peak flows and total ET was due to three soil parameters: hydraulic conductivity KSAT, the percolation controlling parameter SLOPE and the porosity SMCMAX. The vegetation parameterizations with the largest impact were the representation of vegetation density DVEG option 1 (monthly GVF) and the Jarvis stomatal conductance model. The infiltration controlling parameter REFKDT, on which many previous studies focused, impacts peak flows more than total streamflow, but its effect on peak flow is similar or less than the effects of SLOPE, KSAT and SMCMAX in the entire simulation period.

- The impact analysis revealed that the effect of the most important parameters (SLOPE, KSAT, vegetation parameters) on streamflow and ET was similar for all 31 watersheds and in two different hydrological years, indicating the significance of the parameter impact analysis results.
- The Ball-Berry stomatal conductance model, which is the default in Noah-MP LSM, was found to simulate up to 25 % less median transpiration than the Jarvis model. The Jarvis model with the addition of a new equation for nocturnal transpiration simulated total, daytime and nocturnal transpiration close to locally observed amounts. This modification of the Jarvis model was also necessary to obtain acceptable results for streamflow.
- The proposed groundwater loss factor (L_{fac}) in the groundwater bucket component of WRF-Hydro was found to be another useful addition in the model code to reduce the streamflow overestimation by the reduction of baseflow. On average, the median reduction of total streamflow of the 31 watersheds was 30 % in the two calibration years with L_{fac}. The groundwater loss factor can be especially useful for streamflow simulations of ephemeral streams. The inclusion of groundwater losses can be considered to account for the cumulative losses from the water balance of semi-arid Mediterranean watersheds, which are not modeled with WRF-Hydro, such as extractions from groundwater. The groundwater bucket model with the addition of the loss component is useful in simulating an average hydrological behavior of groundwater processes in complex fractured geology, where groundwater basins are not aligned with surface watersheds.
- The grid-based calibration of the distributed model parameters KSAT, SLOPE and REFKDT for 19 spatial classes with PEST proved useful for the estimation of parameter values. The parameters were assigned spatially variable calibrated values in line with their expected hydrologic function on streamflow and spatial variability of land use, topographic slope and geological classes. The advantage of the grid-based calibration is that the calibrated distributed parameters can be used for ungauged streams.
- The final parameterization of WRF-Hydro, based on the results of the grid-based calibration and selection of parameters values and model options from the parameter impact analysis, yielded positive model efficiency (median NSE = 0.49, median KGE = 0.66). The model efficiency was lower, however, in the five-year evaluation period (median NSE = 0.02, median KGE = 0.10). The total streamflow median bias was −5% in calibration period and around 50 % in the evaluation period. The reduction of bias, by about 50 %, is a substantial improvement relative to the baseline parameterization.
- The WRF-Hydro model efficiency metrics and the bias metrics were highest and lowest, respectively, during wet years. The median NSE was about 0.5 for the wettest years, above zero for the medium wet years and about −1 in the driest years. The driest watersheds were also simulated with the highest negative relative biases. The MAE was, however, nearly the same and<0.5 mm/d in both the calibration and in four out of five years in the evaluation period. The overall results imply that the model performance is degraded in years with low total precipitation and dry conditions. Improving the model code by making the surface and stream roughness coefficients time-variant, could potentially improve the model performance for these conditions.
- The calibrated model captures the patterns of the water balance annual partitioning among the components of evaporation, transpiration and interception. The simulated average ET of 31 watersheds for seven years agreed with observations and accounted for 85 % of the input precipitation, which characterizes semi-arid and Mediterranean ecosystems. The runoff coefficients obtained with the calibrated WRF-Hydro model averaged 0.13, whereas those obtained with Noah-MP, which does not simulate lateral flow and re-infiltration, averaged 0.22, compared with the average observed value of 0.14.

Overall, the PEST-based WRF-Hydro calibration for streamflow at multiple watersheds, proved a functional and effective approach for the adjustment of model parameters and equations for both runoff and land surface processes. Additional to the groundwater loss factor and nocturnal transpiration equation, improvements could be made to describe other observed hydrological and ecosystems processes for semi-arid environments and ephemeral streams. The impact of using the grid-based calibrated WRF-Hydro with improved parameterizations on atmospheric modeling could be examined with fully coupled hydrological-atmospheric simulations.

5. Model and data availability:

- The WRF-Hydro model code with the modifications in the Jarvis stomatal conductance model and in the groundwater bucket model used in this study is publicly available at: https://doi.org/10.5281/zenodo.7335585
- WRF model: https://github.com/wrf-model/WRF
- WRF-Hydro model: https://github.com/NCAR/wrf_hydro_nwm_public
- ArcGIS preprocessing tool: https://github.com/NCAR/wrf_hydro_arcgis_preprocessor
- DEM and geology data: https://www.moa.gov.cy/moa/gsd/gsd.nsf
- Copernicus satellite LAI: https://land.copernicus.eu/
- Corine Land Cover: https://land.copernicus.eu/

CRediT authorship contribution statement

Ioannis Sofokleous: Conceptualization, Data curation, Formal analysis, Methodology, Investigation, Software, Validation, Writing – original draft, Writing – review & editing. **Adriana Bruggeman:** Conceptualization, Methodology, Investigation, Writing – review & editing. **Corrado Camera:** Methodology, Software, Writing – review & editing. **Marinos Eliades:** Methodology, Writing – review & editing.

Declaration of Competing Interest

The authors declare that they have no known competing financial interests or personal relationships that could have appeared to influence the work reported in this paper.

Acknowledgments:

The authors would like to thank The Cyprus Institute for the support of the research presented in this paper. We would also like to thank the Water Development Department of Cyprus and the Department of Meteorology of Cyprus for provision of streamflow and precipitation observational data, as well as Thekla Loizou and Panayiotis Vorkas of the High Performance Computing Facility of The Cyprus Institute for the assistance with the installation of the models used in this study.

Appendix A. The Jarvis stomatal resistance model

An empirical formula for the stomatal resistance was proposed by Jarvis (1976), which is still widely used. The formula computes, according to Chen et al. (1996), the canopy stomatal resistance r_s at any environmental condition.

$$r_s = rs_{min} \bullet (F_1F_2F_3F_4)^{-1} \quad (A.1)$$

Given the minimum stomatal resistance (rs_{min}), corresponding to the value of canopy resistance at optimal environmental conditions for transpiration, the Jarvis model suggests four stress functions, F_1, F_2, F_3 and F_4, ranging from 0 to 1, to adjust rs_{min}. The functions represent the effects of solar radiation (F_1), vapor pressure deficit (F_2), canopy air temperature (F_3) and soil moisture (F_4) on transpiration with the following equations:

$$F_1 = \frac{r_{smin}/r_{smax} + f}{1 + f} \text{ where } f = 0.55\frac{R_s}{R_{gl}}\frac{2}{LAI} \quad (A.2)$$

$$F_2 = \frac{1}{1 + b[q_{sat}(T) - q(T)]} \quad (A.3)$$

$$F_3 = 1 - B(Topt - T)^2 \quad (A.4)$$

$$F_4 = \sum_{i}^{nroot} \frac{(\theta i - \theta_w)\Delta_{zi}}{(\theta_{ref} - \theta_w)z_{root.i}} \quad (A.5)$$

where each of the four functions is related to the variables of intensity of direct solar radiation R_s (Wm^{-2}), the vapor pressure deficit q_{sat} - q (kg/kg), the canopy air temperature T (K) and the volumetric soil moisture content θ_i (m^3/m^3) in soil layer with depth Δz (m) and with vegetation depth of roots z_{root} (m), for n_{root} number of soil layers with roots.

The four stress functions contain parameters that are either measurable or estimated through a fitting process of the Jarvis based stomatal resistance against actual measurements. The fitting parameters and the model default values are: the maximum canopy resistance r_{smax}, which corresponds to the cuticular resistance of the leaves and a value of 5000 sm^{-1} is a representative value for many trees (Dickinson 1984), the fitting parameter R_{gl} for the radiation response (F_1), ranging between 30 and 100 Wm^{-2} and can be vegetation specific (Noilhan and Planton, 1989), the fitting parameter for the vapor pressure deficit response (F_2), ranging from 36 to 56 (Chen et al., 1996), the fitting parameter B for the temperature response (F_3), suggested to be 0.0016 (Dickinson 1984) and the parameter T_{opt}, the optimal transpiration temperature equal to 298 K (Dickinson 1984), which is replaced by 293 K in this study for the case of woody Mediterranean vegetation, i.e, trees and shrubs (Larcher 1995) and crops (Wang et al., 2017). Other parameters are the vegetation type specific Leaf Area Index (LAI; m^2/m^2) and the soil texture specific wilting point θ_w (-) and field capacity θ_{ref} (-).

Appendix B. Land use classes and leaf area indices

Table B1
Noah-MP prescribed monthly Leaf Area Index (LAI), monthly field (pixel) average LAI for the land use categories in 31 watersheds in Cyprus and the corresponding land surface class per land use used for the calibration of REFKDT parameter.

CLC Land use category	Coniferous forest	Mixed Forests	Sclerophyllous vegetation	Natural grassland	Annual & Permanent Crops	Urban	Vineyards, Fruit trees, Mixed Agriculture & natural vegetation	Bare rock, sparsely vegetated areas
USGS Land use category	1. Evergreen needle leaf forest	5. Mixed Forests	6. Closed shrubland	10. Grasslands	12. Cropland	13. Urban and Built-Up	14. Cropland/Natural vegetation mosaic	16. Barren or Sparsely Vegetated
Coverage (%)	46.0	2.7	18.5	2.8	12.1	0.3	16.5	1.2
Land Surface Unit	1,2,3	1,2,3	4,5,6	4,5,6	7,8,9	7,8,9	7,8,9	7,8,9
Noah MP prescribed LAI (m^2/m^2)								
Jan	4	2	0	0.4	0	0	0.2	0
Feb	4	2	0	0.5	0	0	0.3	0
Mar	4	2.2	0.3	0.6	0	0	0.3	0
Apr	4	2.6	0.9	0.7	0	0	0.4	0
May	4	3.5	2.2	1.2	1	0	1.1	0
Jun	4	4.3	3.5	3	2	0	2.5	0
Jul	4	4.3	3.5	3.5	3	0	3.2	0
Aug	4	3.7	2.5	1.5	3	0	2.2	0
Sep	4	2.6	0.9	0.7	1.5	0	1.1	0
Oct	4	2.2	0.3	0.6	0	0	0.3	0
Nov	4	2	0	0.5	0	0	0.3	0
Dec	4	2	0	0.4	0	0	0.2	0
Copernicus Global Land Service LAI (m^2/m^2) (pixel average)								
Jan	1.3	0.9	1.1	1.3	1.4	0.9	1.1	0.9
Feb	1.3	1.2	1.2	1.6	1.8	1.2	1.4	1.0
Mar	1.3	1.1	1.1	1.4	1.2	0.8	1.2	0.8
Apr	1.2	0.9	0.9	0.8	0.8	0.3	0.9	0.5
May	1.2	0.8	0.8	0.4	0.6	0.3	0.6	0.4
Jun	1.2	0.6	0.8	0.4	0.5	0.3	0.6	0.4
Jul	1.1	0.5	0.7	0.3	0.4	0.2	0.5	0.3
Aug	1.1	0.5	0.7	0.3	0.3	0.2	0.4	0.3
Sep	1.1	0.5	0.7	0.3	0.3	0.2	0.4	0.3
Oct	1.2	0.7	0.8	0.3	0.3	0.2	0.4	0.3
Nov	1.2	1.0	1.0	0.5	0.5	0.3	0.6	0.5
Dec	1.2	1.2	1.1	1.0	1.0	0.7	1.1	0.7

Appendix C. Hydrographs

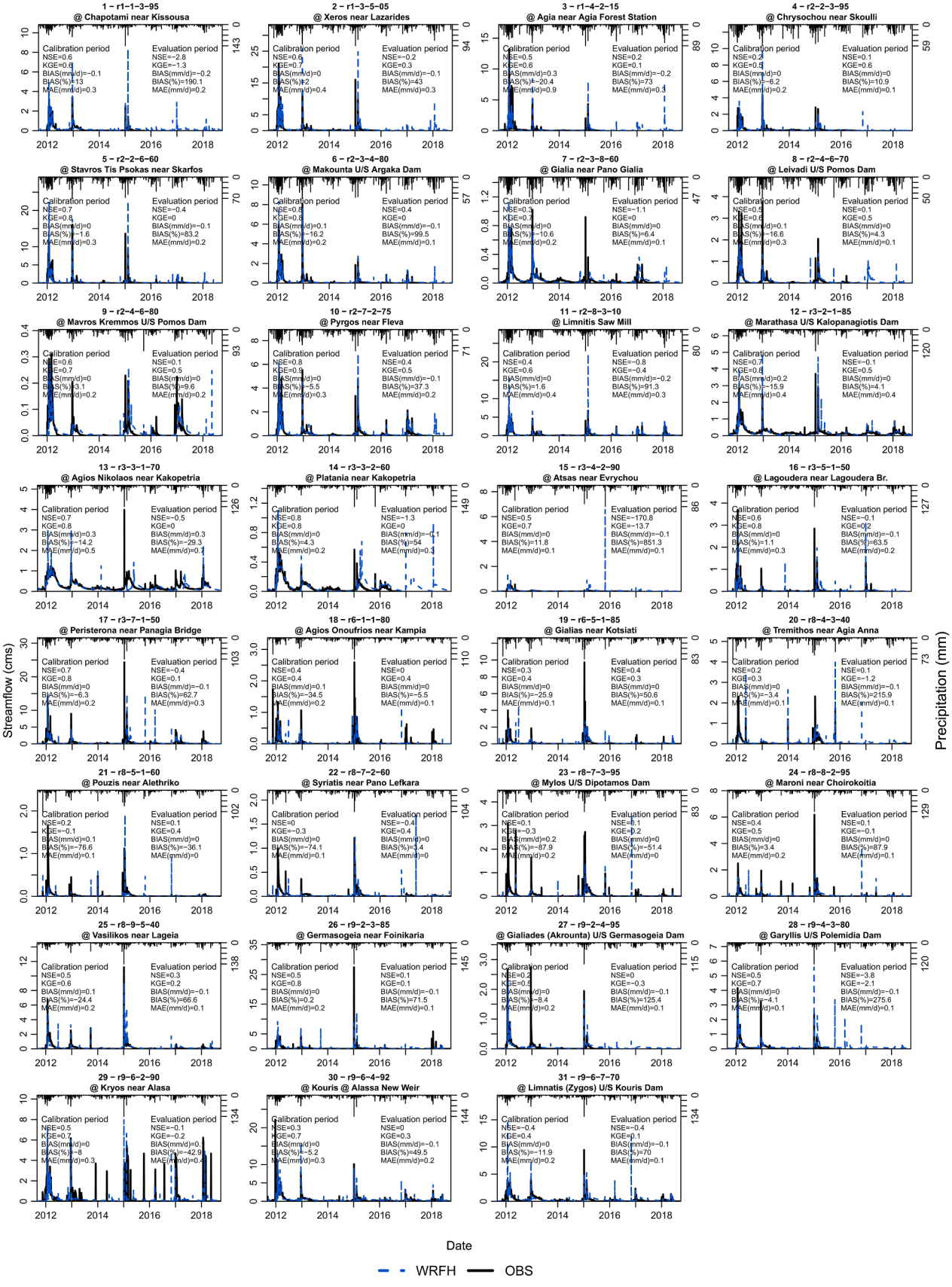

Fig. C1. Hydrographs of WRF-Hydro simulated streamflow and observed streamflow (m^3s^{-1}) at 31 watersheds with evaluation metrics for the calibration period (2011–2013) and the evaluation period.

Appendix D. WRF-Hydro dam parameters

Table D1
Dam information, obtained from the Water Development of Cyprus and WRF-Hydro dam parameters for the routing grid of Troodos study area.

Code	Reservoir name	Station downstream	Capacity (10^3m^3)	LkArea[1] (m^2)	Spillway height (m)	Initial fractional storage
d2-8-1	TSAKISTRA	r2-8-3-10	100	4348	23	0.60
d6-5-1-lw	LYTHRODONTAS 2	r6-5-1-85	32	2909	11	0.33
d6-5-1-up	LYTHRODONTAS 1	r6-5-1-85	32	3200	10	0.83
d8-4-1-61	LYMPIA	r8-4-3-40	220	18,333	12	0.81
d8-7-2-05	LEFKARA	r8-7-2-60	13,850	195,070	71	0.27
d8-9-1	AYIOI VAVATSINIAS	r8-9-5-40	530	27,895	19	0.50
d9-2-1-85	ARAKAPAS	r9-2-3-85	129	5609	23	0.83
d9-6-1-60	PERA-PEDI	r9-6-2-90	55	2500	22	1
d9-6-3-75	TRIMIKLINI	r9-6-4-92	340	10,303	33	0.41

1 The value of the generated parameter for the dam surface area in the gridded domain (LkArea) by the WRF-Hydro GIS pre-processor was modified so that the product LkArea times Spillway height equals the actual volume (storage capacity) of the dam.

Appendix E. Model performance evaluation equations

The Nash-Sutcliffe Efficiency (NSE; Nash and Sutcliffe, 1970) ranges between -∞ and 1.0 and when NSE equals 1, a perfect fit of the simulated data to the observed data is denoted. The equation for NSE is:

$$NSE = 1 - \left[\frac{\sum_{i=1}^{n}\left(Y_i^{obs} - Y_i^{sim}\right)^2}{\sum_{i=1}^{n}\left(Y_i^{obs} - \bar{Y^{obs}}\right)^2}\right] \quad (E.1)$$

where Y^{obs} and Y^{sim} are the observed and modeled streamflow respectively at time step i and n is the total number of time steps. Kling-Gupta Efficiency (KGE; Kling et al., 2012) has the same range as NSE and the perfect fit of simulated to the observed streamflow is achieved when KGE equals 1. The equation for KGE is:

$$KGE = 1 - \sqrt{(r-1)^2 + (\beta-1)^2 + (\gamma-1)^2} \quad (E.2)$$

$$\beta = \frac{Q_{sim}}{\overline{Q_{obs}}}$$

$$\gamma = \frac{\sigma_{sim}/Q_{sim}}{\overline{\sigma_{obs}/Q_{obs}}}$$

where r is the linear correlation coefficient between simulated and observed flows, Q_{sim} and Q_{obs} are the mean simulated and observed flow respectively and σ_{sim} and σ_{obs} are the standard deviations of simulated and observed runoff respectively.

References

Arnault, J., Wagner, S., Rummler, T., Fersch, B., Bliefernicht, J., Andresen, S., Kunstmann, H., 2015. Role of runoff–infiltration partitioning and resolved overland flow on land–atmosphere feedbacks: A case study with the WRF-Hydro coupled modelling system for West Africa. J. Hydrometeorol. 17 (5), 1489–1516. https://doi.org/10.1175/JHM-D-17-0042.1.

Arnault, J., Rummler, T., Baur, F., Lerch, S., Wagner, S., Fersch, B., Zhang, Z., Kerandi, N., Keil, C., Kunstmann, H., 2018. Precipitation sensitivity to the uncertainty of terrestrial water flow in WRF-Hydro–An ensemble analysis for Central Europe. J. Hydrometeorol. 19 (6), 1007–1025. https://doi.org/10.1175/JHM-D-15-0089.1.

Arsenault, K.R., Nearing, G.S., Wang, S., Yatheendradas, S., Peters-Lidard, C.D., 2018. Parameter sensitivity of the Noah-MP land surface model with dynamic vegetation. J. Hydrometeorol. 19 (5), 815–830. https://doi.org/10.1175/jhm-d-17-0205.1.

Ball, J.T., Woodrow, I.E., Berry, J.A., 1987. A model predicting stomatal conductance and its contribution to the control of photosynthesis under different environmental conditions.. In: Process in Photosynthesis Research, 1. Martinus Nijhoff, Dordrecht, Netherlands, pp. 221–234. https://doi.org/10.1007/978-94-017-0519-6_48.

Boronina, A., Renard, P., Balderer, W., Christodoulides, A., 2003. Groundwater resources in the Kouris catchment (Cyprus): data analysis and numerical modelling. J. Hydrol. 271 (1–4), 130–149. https://doi.org/10.1016/S0022-16949(02)00322-0.

Camera, C., Bruggeman, A., Hadjinicolaou, P., Pashiardis, S., Lange, M.A., 2014. Evaluation of interpolation techniques for the creation of gridded daily precipitation (1× 1 km2); Cyprus, 1980–2010. J. Geophys. Res.-Atmos. 119 (2), 693–712. https://doi.org/10.1002/2013JD020611.

Camera, C., Zomeni, Z., Noller, J.S., Zissimos, A.M., Christoforou, I.C., Bruggeman, A., 2017. A high resolution map of soil types and physical properties for Cyprus: A digital soil mapping optimization. Geoderma 285, 35–49. https://doi.org/10.1016/j.geoderma.2016.09.019.

Camera, C., Bruggeman, A., Zittis, G., Sofokleous, I., Arnault, J., 2020. Simulation of extreme rainfall and streamflow events in small Mediterranean watersheds with a one-way-coupled atmospheric–hydrologic modelling system. Nat. Hazard. Earth Sys. 20 (10), 2791–2810. https://doi.org/10.5194/nhess-20-2791-2020.

Chen, F., Mitchell, K., Schaake, J., Xue, Y., Pan, H.L., Koren, V., Duan, Q.Y., Ek, M., Betts, A., 1996. Modelling of land surface evaporation by four schemes and comparison with FIFE observations. J. Geophys. Res.-Atmos. 101 (D3), 7251–7268. https://doi.org/10.1029/95JD02165.

Christofi, C., Bruggeman, A., Kuells, C., Constantinou, C., 2020. Hydrochemical evolution of groundwater in gabbro of the Troodos Fractured Aquifer. A comprehensive approach. Appl. Geochem. 114, 104524. https://doi.org/10.1016/j.apgeochem.2020.104524.

Cuntz, M., Mai, J., Samaniego, L., Clark, M., Wulfmeyer, V., Branch, O., Attinger, S., Thober, S., 2016. The impact of standard and hard-coded parameters on the hydrologic fluxes in the Noah-MP land surface model. J. Geophys. Res. Atmos. 121 (18), 10–676. https://doi.org/10.1002/2016JD025097.

Dickinson, R.E., 1984. Modelling evapotranspiration for three-dimensional global climate models. Climate processes and climate sensitivity 29, 58–72. https://doi.org/10.1029/GM029p0058.

Doherty, J., 2015. Calibration and uncertainty analysis for complex environmental models. Watermark Numerical Computing, Brisbane, Australia.

Doherty J., 2020. Model-Independent Parameter Estimation User Manual Part I: PEST, SENSAN and Global Optimisers, Watermark Numerical Computing, Brisbane, Australia, Available online at: https://pesthomepage.org/documentation.

Ek, M.B., Mitchell, K.E., Lin, Y., Rogers, E., Grunmann, P., Koren, V., Gayno, G., Tarpley, J.D., 2003. Implementation of Noah land surface model advances in the

National Centers for Environmental Prediction operational mesoscale Eta model. J. Geophys. Res. Atmos. 108 (D22) https://doi.org/10.1029/2002JD003296.
Eliades, M., Bruggeman, A., Djuma, H., Lubczynski, M.W., 2018a. Tree water dynamics in a semi-arid. Pinus brutia forest. Water 10 (8), 1039. https://doi.org/10.3390/w10081039.
Eliades, M., Bruggeman, A., Lubczynski, M.W., Christou, A., Camera, C., Djuma, H., 2018b. The water balance components of Mediterranean pine trees on a steep mountain slope during two hydrologically contrasting years. J. Hydrol. 562, 712–724. https://doi.org/10.1016/j.jhydrol.2018.05.048.
Eliades, M., Bruggeman, A., Djuma, H., Christou, A., Rovanias, K., Lubczynski, M.W., 2022. Testing three rainfall interception models and different parameterization methods with data from an open Mediterranean pine forest. Agr. Forest Meteorol. 313, 108755. https://doi.org/10.1016/j.agrformet.2021.108755.
Fang, L., Zhan, X., Hain, C.R., Yin, J., Liu, J., 2018. Impact of GVF Derivation Methods on Noah Land Surface Model Simulations and WRF Model Forecasts. J. Hydrometeorol. 19 (12), 1917–1933. https://doi.org/10.1175/JHM-D-18-0075.1.
Fersch, B., Senatore, A., Adler, B., Arnault, J., Mauder, M., Schneider, K., Völksch, I., Kunstmann, H., 2020. High-resolution fully coupled atmospheric–hydrological modeling: a cross-compartment regional water and energy cycle evaluation. Hydrol. Earth Sys. 24 (5), 2457–2481. https://doi.org/10.5194/hess-24-2457-2020.
Gigante, V., Iacobellis, V., Manfreda, S., Milella, P., Portoghese, I., 2009. Influences of Leaf Area Index estimations on water balance modeling in a Mediterranean semi-arid basin. Nat. Hazard. Earth Sys. 9 (3), 979–991. https://doi.org/10.5194/nhess-9-979-2009.
Givati, A., Gochis, D., Rummler, T., Kunstmann, H., 2016. Comparing One-Way and Two-Way Coupled Hydrometeorological Forecasting Systems for Flood Forecasting in the Mediterranean Region. Hydrology 3 (2), 19. https://doi.org/10.3390/hydrology3020019.
Gochis, D.J., M. Barlage, A. Dugger, K. FitzGerald, L. Karsten, M. McAllister, J. McCreight, J. Mills, A. RafieeiNasab, L. Read, K. Sampson, D. Yates, W. Yu, 2018. The WRF-Hydro modelling system technical description, (Version 5.0) NCAR Technical Note, NCAR, Boulder, CO, USA, Available online at: https://ral.ucar.edu/projects/wrf_hydro/technical-description-user-guide.
Gutman, G., Ignatov, A., 1998. The derivation of the green vegetation fraction from NOAA/AVHRR data for use in numerical weather prediction models. Int. J. Remote Sens. 19 (8), 1533–1543. https://doi.org/10.1080/014311698215333.
Hargreaves, G.H., Samani, Z.A., 1985. Reference crop evapotranspiration from temperature. Appl. Eng. Agric. 1 (2), 96–99. https://doi.org/10.13031/2013.26773.
Hundecha, Y., Bárdossy, A., 2004. Modelling of the effect of land use changes on the runoff generation of a river basin through parameter regionalization of a watershed model. J. Hydrol. 292 (1–4), 281–295. https://doi.org/10.1016/j.jhydrol.2004.01.002.
Ingwersen, J., Imukova, K., Högy, P., Streck, T., 2015. On the use of the post-closure methods uncertainty and to evaluate the performance of land surface models against eddy covariance flux data. Biogeosciences 12 (8), 2311–2326. https://doi.org/10.5194/bg-12-2311-2015.
Jarvis, P.G., 1976. The interpretation of the variations in leaf water potential and stomatal conductance found in canopies in the field. Philos. Trans. R. Soc. London. Series B, Biological Sci. 273 (927), 593–610. https://doi.org/10.1098/rstb.1976.0035.
Kling, H., Fuchs, M., Paulin, M., 2012. Runoff conditions in the upper Danube basin under an ensemble of climate change scenarios. J. Hydrol. 424–425, 264. https://doi.org/10.1016/j.jhydrol.2012.01.011.
Larcher, W., 1995. Physiological Plant Ecology, 3rd ed.,. Springer-Verland, Berlin, Germany. 506,.
Li, J., Chen, F., Lu, X., Gong, W., Zhang, G., Gan, Y., 2020. Quantifying contributions of uncertainties in physical parameterization schemes and model parameters to overall errors in Noah-MP dynamic vegetation modeling. J. Adv. Model. Earth Syst. 12 (7) https://doi.org/10.1029/2019MS001914.
Lin, T.S., Cheng, F.Y., 2016. Impact of soil moisture initialization and soil texture on simulated land–atmosphere interaction in Taiwan. J. Hydrometeorol 17 (5), 1337–1355. https://doi.org/10.1175/JHM-D-15-0024.1.
Maxwell, R.M., Chow, F.K., Kollet, S.J., 2007. The groundwater–land-surface–atmosphere connection: Soil moisture effects on the atmospheric boundary layer in fully-coupled simulations. Adv. Water Resour. 30 (12), 2447–2466. https://doi.org/10.1016/j.advwatres.2007.05.018.
Maxwell, R.M., Lundquist, J.K., Mirocha, J.D., Smith, S.G., Woodward, C.S., Tompson, A. F., 2011. Development of a coupled groundwater–atmosphere model. Mon. Weather Rev. 139 (1), 96–116. https://doi.org/10.1175/2010MWR3392.1.
Nash, J.E., Sutcliffe, J.V., 1970. River flow forecasting through conceptual models part I – A discussion of principles. J. Hydrol. 10 (3), 282–290. https://doi.org/10.1016/0022-1694(70)90255-6.
Niu, G.-Y., Yang, Z.-L., Mitchell, K.E., Chen, F., Ek, M.B., Barlage, M., Kumar, A., Manning, K., Niyogi, D., Rosero, E., Tewari, M., Xia, Y., 2011. The community Noah land surface model with multiparameterization options (Noah-MP): 1. Model description and evaluation with local-scale measurements. J. Geophys. Res. 116 (D12) https://doi.org/10.1029/2010JD015139.
NOAA (National Oceanic and Atmospheric Administration), 2016. National Water Model: Improving NOAA's Water Prediction Services. Available online at: http://water.noaa.gov/documents/wrn-national-water-model.pdf.
Noilhan, J., Planton, S., 1989. A simple parameterization of land surface processes for meteorological models. Mon. Weather Rev. 117 (3), 536–549. https://doi.org/10.1175/1520-0493(1989)117%3C0536:ASPOLS%3E2.0.CO;2.
Norman, J.M., Kustas, W.P., Humes, K.S., 1995. Source approach for estimating soil and vegetation energy fluxes in observations of directional radiometric surface temperature. Agric. Forest Meteorol. 77 (3–4), 263–293. https://doi.org/10.1016/0168-1923(95)02265-Y.
Pineda, N., Jorba, O., Jorge, J., Baldasano, J.M., 2004. Using NOAA AVHRR and SPOT VGT data to estimate surface parameters: application to a mesoscale meteorological model. Int. J. Remote Sens. 25 (1), 129–143. https://doi.org/10.1080/0143116031000115201.
Rummler, T., Arnault, J., Gochis, D., Kunstmann, H., 2019. Role of lateral terrestrial water flow on the regional water cycle in a complex terrain region: Investigation with a fully coupled model system. J. Geophys. Res.-Atmos. 124 (2), 507–529. https://doi.org/10.1029/2018JD029004.
Rummler, T., Wagner, A., Arnault, J., Kunstmann, H., 2022. Lateral terrestrial water fluxes in the LSM of WRF-Hydro: Benefits of a 2D groundwater representation. Hydrol. Processes 36 (3), 14510. https://doi.org/10.1002/hyp.14510.
Rutledge, A.T., 1998. Computer programs for describing the recession of ground-water discharge and for estimating mean ground-water recharge and discharge from streamflow data. US Geological Survey Water-Resources Investigations Report 98-4148, 43.
Schaller, M.F., Fan, Y., 2009. River basins as groundwater exporters and importers: Implications for water cycle and climate modeling. Geophys. Res. Atmos. 114 (D4) https://doi.org/10.1029/2008JD010636.
Senatore, A., Mendicino, G., Gochis, D.J., Yu, W., Yates, D.N., Kunstmann, H.G., 2015. Fully coupled atmosphere-hydrology simulations for the central Mediterranean: Impact of enhanced hydrological parameterization for short and long time scales. J. Adv. Model. Earth Syst. 7 (4), 1693–1715. https://doi.org/10.1002/2015MS000510.
Skamarock, W. C., and Coauthors, 2019. A Description of the Advanced Research WRF Model, Version 4.1 (No. NCAR/TN-556+STR), Boulder, CO, USA, Available online at: https://opensky.ucar.edu/islandora/object/opensky:2898.
Silver, M., Karnieli, A., Ginat, H., Meiri, E., Fredj, E., 2017. An innovative method for determining hydrological calibration parameters for the WRF-Hydro model in arid regions. Environ. Model. Softw. 91, 47–69. https://doi.org/10.1016/j.envsoft.2017.01.010.
Sofokleous, I., Bruggeman, A., Michaelides, S., Hadjinicolaou, P., Zittis, G., Camera, C., 2021. Comprehensive Methodology for the Evaluation of High-Resolution WRF Multiphysics Precipitation Simulations for Small. Topographically Complex Domains. J. Hydrometeorol. 22 (5), 1169–1186. https://doi.org/10.1175/JHM-D-20-0110.1.
Udluft, P., Dünkeloh, A., Mederer, J., Kulls, C., Schaller, J., 2006. Re-evaluation of the groundwater resources of Cyprus - GRC project report. Geological Survey Department of Cyprus, Nicosia, Cyprus.
Wang, H., Guan, H., Liu, N., Soulsby, C., Tetzlaff, D., Zhang, X., 2020. Improving the Jarvis-type model with modified temperature and radiation functions for sap flow simulations. J. Hydrol. 587, 124981. https://doi.org/10.1016/j.jhydrol.2020.124981.
Wang, E., Martre, P., Zhao, Z., Ewert, F., Maiorano, A., Rötter, R.P., Kimball, B.A., Ottman, M.J., Wall, G.W., White, J.W., Reynolds, M.P., 2017. The uncertainty of crop yield projections is reduced by improved temperature response functions. Nat. Plants 3 (8), 1–13. https://doi.org/10.1038/nplants.2017.102.
Whitley, R., Medlyn, B., Zeppel, M., Macinnis-Ng, C., Eamus, D., 2009. Comparing the Penman-Monteith equation and a modified Jarvis-Stewart model with an artificial neural network to estimate stand-scale transpiration and canopy conductance. J. Hydrol. 373 (1–2), 256–266. https://doi.org/10.1016/j.jhydrol.2009.04.036.
Yang, Z.L., Niu, G.Y., Mitchell, K.E., Chen, F., Ek, M.B., Barlage, M., Longuevergne, L., Manning, K., Niyogi, D., Tewari, M., Xia, Y., 2011. The community Noah land surface model with multiparameterization options (Noah-MP): 2. Evaluation over global river basins. J. Geophys. Res. Atmos. 116 (D12) https://doi.org/10.1029/2010JD015140.
Yucel, I., Onen, A., Yilmaz, K.K., Gochis, D.J., 2015. Calibration and evaluation of a flood forecasting system: Utility of numerical weather prediction model, data assimilation and satellite-based rainfall. J. Hydrol. 523, 49–66. https://doi.org/10.1016/j.jhydrol.2015.01.042.
Zhang, J., Lin, P., Gao, S., Fang, Z., 2020. Understanding the re-infiltration process to simulating streamflow in North Central Texas using the WRF-hydro modelling system. J. Hydrol. 587, 124902. https://doi.org/10.1016/j.jhydrol.2020.124902.
Zheng, H., Yang, Z.L., Lin, P., Wei, J., Wu, W.Y., Li, L., Zhao, L., Wang, S., 2019. On the sensitivity of the precipitation partitioning into evapotranspiration and runoff in land surface parameterizations. Water Resour. Res. 55 (1), 95–111. https://doi.org/10.1029/2017WR022236.
Zoumides, C., Bruggeman, A., Giannakis, E., Camera, C., Djuma, H., Eliades, M., Charalambous, K., 2017. Community-based rehabilitation of mountain terraces in Cyprus. Land Degrad. Dev. 28 (1), 95–105. https://doi.org/10.1002/ldr.2586.